# Supplement to:

# State of Wildfires 2025-2026

Chantelle Burton[1,★], Francesca Di Giuseppe[2,★], Matthew W. Jones[3,★], Douglas I. Kelley[4,★] et al.

Correspondence to:
chantelle.burton@metoffice.gov.uk
Francesca.DiGiuseppe@ecmwf.int
matthew.w.jones@uea.ac.uk
doukel@ceh.ac.uk

# S1. Methods and Evaluation

## S1.1. Hydroclimatic Drivers

**Table S1:** Input features used to derive hydroclimatic anomalies and the driver attribution in PoF. In some cases, native data was regridded from higher resolution to coarse resolution for use in the model.

| Variable | Category | Source | Reference |
|---|---|---|---|
| High Vegetation Cover | Fuel | CONFESS | Boussetta et al., 2021 |
| Low Vegetation Cover | Fuel | CONFESS | Boussetta et al., 2021 |
| Type of High Vegetation | Fuel | CONFESS | Boussetta et al., 2021 |
| Type of Low Vegetation | Fuel | CONFESS | Boussetta et al., 2021 |
| High Vegetation LAI | Fuel | CGLS | Copernicus Global Land Service, 2026 |
| Low Vegetation LAI | Fuel | CGLS | Copernicus Global Land Service, 2026 |
| Dead Foliage Load | Fuel | Sparky-Fuel | McNorton & Di Giuseppe, 2024 |
| Dead Wood Load | Fuel | Sparky-Fuel | McNorton & Di Giuseppe, 2024 |
| Live Leaf Load | Fuel | Sparky-Fuel | McNorton & Di Giuseppe, 2024 |
| Live Wood Load | Fuel | Sparky-Fuel | McNorton & Di Giuseppe, 2024 |
| Dead Foliage Moisture | Fuel | Sparky-Fuel | McNorton & Di Giuseppe, 2024 |
| Dead Wood Moisture | Fuel | Sparky-Fuel | McNorton & Di Giuseppe, 2024 |
| Live Fuel Moisture | Fuel | Sparky-Fuel | McNorton & Di Giuseppe, 2024 |
| 2m Temperature | Weather | ERA5 Land | Muñoz-Sabater et al., 2021 |
| Wind Speed | Weather | ERA5 Land | Muñoz-Sabater et al., 2021 |
| Relative Humidity | Weather | ERA5 Land | Muñoz-Sabater et al., 2021 |
| Total Precipitation | Weather | ERA5 Land | Muñoz-Sabater et al., 2021 |
| Orography | | ECLand | Boussetta et al., 2021 |
| Population Density | Ign-Supp | GPW v4 – SEDAC | CIESIN, 2017 |
| Nightlights | Ign-Supp | Harmonized Global Nighttime Light | Li et al., 2020 |
| Gross Domestic Product | Ign-Supp | Our World in Data | Kummu et al., 2025 |
| Human Development Index | Ign-Supp | UNDP Human Development Report | Liu et al., 2024 |
| Road Density | Ign-Supp | Global Roads Inventory Dataset | Meijer et al., 2018 |
| Terrestrial Biome Protection | Ign-Supp | EPI - Yale | Block et al., 2024 |
| Government Effectiveness | Ign-Supp | Our World in Data | World Bank, 2025 |
| Urban Cover | Ign-Supp | GHSL | Pesaresi & Politis, 2025 |
| Lightning | Ign-Supp | IFS | Lopez, 2016 |

## S1.2. Influence of Climate Change on Focal Events

### S1.2.1. Attribution of Present Day Focal Events - FWI

For the FWI WWA multi-model analysis, we assess the performance of each climate model dataset regionally using a qualitative comparison of the seasonal cycle and spatial pattern for a 1990-2019 climatology, and the parameters of the fitted statistical models. Each of these three criteria were rated as ‘good’, ‘reasonable’ or ‘bad’ – with a model rated as ‘good’ if ‘good’ in all three properties, ‘bad’ if ‘bad’ in any property, and ‘reasonable’ otherwise. Whilst we would ideally only use ‘good’ models, the low number of these meant that ‘reasonable’ models were also considered. We show the full model evaluation in the tables below.

**Table S2: Model evaluation for FWI95 – Midwest Canadian Forest Shield.** Evaluation results of the climate models considered for attribution analysis of FWI95 in the Midwest Canadian Forest Shield region. For each model, the best estimates of the Scale and Shape parameters of the GEV are shown, along with 95% confidence intervals. If the best estimate of these parameters falls within the 95% CI for the reanalysis, the model was evaluated as good; else if the 95% CIs of the model and reanalysis overlapped it was rated as reasonable; and otherwise was rated as a bad representation of the extreme FWI95 distribution. Furthermore evaluation of the seasonal cycle and spatial pattern are shown, which were evaluated by visual comparison of the seasonal and geospatial climatology to reanalysis patterns – comparison figures available on zenodo. The lowest realisation member of each model with all “good” ratings was included in the final analysis, if there was no realisation meeting that criteria, the lowest overall “reasonable” model was included.

| | | | | **Scale parameter Obs Min: 0.151 Obs Max: 0.303** | | | **Shape parameter Obs Min: -0.553 Obs Max: -0.0322** | | | | | | |
|---|---|---|---|---|---|---|---|---|---|---|---|---|---|
| **Model** | **Member** | **Seasonal cycle** | **Spatial pattern** | Best estimate | Lower bound | Upper bound | Best estimate | Lower bound | Upper bound | **Sigma** | **Shape** | **Rating** | **Model Inclusion** |
| AWI-ESM-1-REcoM | r1i1p1f1 | bad | good | 0.419 | 0.331 | 0.476 | -0.131 | -0.578 | 0.277 | bad | good | bad | **N** |
| CanESM5 | r1i1p2f1 | good | good | 0.174 | 0.129 | 0.201 | 0.060 | -0.200 | 0.427 | good | reasonable | reasonable | **N** |
| CanESM5 | r8i1p1f1 | good | good | 0.182 | 0.138 | 0.213 | -0.068 | -0.332 | 0.217 | good | good | good | **Y** |
| CNRM-CM6-1-HR | r1i1p1f2 | reasonable | good | 0.206 | 0.163 | 0.238 | -0.340 | -0.645 | -0.121 | good | good | reasonable | **N** |
| CNRM-CM6-1 | r1i1p1f2 | reasonable | good | 0.201 | 0.160 | 0.230 | -0.219 | -0.475 | 0.043 | good | good | reasonable | **N** |
| CNRM-ESM2-1 | r1i1p1f2 | reasonable | good | 0.164 | 0.129 | 0.195 | -0.545 | -0.764 | -0.389 | good | good | reasonable | **Y** |
| GFDL-CM4 | r1i1p1f1 | good | good | 0.164 | 0.126 | 0.190 | 0.281 | -0.186 | 0.575 | good | reasonable | reasonable | **Y** |
| INM-CM4-8 | r1i1p1f1 | bad | reasonable | 0.315 | 0.261 | 0.352 | 0.037 | -0.179 | 0.248 | reasonable | reasonable | bad | **N** |
| INM-CM5-0 | r1i1p1f1 | bad | reasonable | 0.307 | 0.214 | 0.349 | 0.001 | -0.156 | 0.277 | reasonable | reasonable | bad | **N** |
| MIROC6 | r1i1p1f1 | good | reasonable | 0.116 | 0.089 | 0.136 | -0.136 | -0.426 | 0.068 | bad | good | bad | **N** |
| MIROC6 | r2i1p1f1 | good | reasonable | 0.138 | 0.112 | 0.157 | -0.155 | -0.428 | 0.068 | reasonable | good | reasonable | **Y** |
| MIROC6 | r3i1p1f1 | good | reasonable | 0.157 | 0.116 | 0.185 | -0.303 | -0.716 | -0.166 | good | good | reasonable | **N** |
| MPI-ESM1-2-LR | r10i1p1f1 | reasonable | reasonable | 0.403 | 0.327 | 0.461 | 0.184 | -0.064 | 0.423 | bad | reasonable | bad | **N** |
| MPI-ESM1-2-LR | r11i1p1f1 | reasonable | reasonable | 0.305 | 0.234 | 0.361 | -0.158 | -0.382 | 0.018 | reasonable | good | reasonable | **N** |
| MPI-ESM1-2-LR | r12i1p1f1 | reasonable | reasonable | 0.275 | 0.216 | 0.319 | 0.321 | 0.091 | 0.550 | good | reasonable | reasonable | **N** |
| MPI-ESM1-2-LR | r13i1p1f1 | good | bad | 0.318 | 0.241 | 0.358 | 0.002 | -0.310 | 0.376 | reasonable | reasonable | bad | **N** |
| MPI-ESM1-2-LR | r14i1p1f1 | reasonable | bad | 0.397 | 0.293 | 0.463 | 0.042 | -0.113 | 0.280 | reasonable | reasonable | bad | **N** |
| MPI-ESM1-2-LR | r15i1p1f1 | good | bad | 0.358 | 0.291 | 0.406 | 0.033 | -0.182 | 0.196 | reasonable | reasonable | bad | **N** |

| | | | | | | | | | | | | | |
|---|---|---|---|---|---|---|---|---|---|---|---|---|---|
| MPI-ESM1-2-LR | r16i1p1f1 | good | bad | 0.272 | 0.214 | 0.312 | 0.233 | 0.028 | 0.492 | good | reasonable | bad | **N** |
| MPI-ESM1-2-LR | r17i1p1f1 | reasonable | bad | 0.344 | 0.268 | 0.395 | 0.113 | -0.098 | 0.357 | reasonable | reasonable | bad | **N** |
| MPI-ESM1-2-LR | r18i1p1f1 | reasonable | bad | 0.302 | 0.214 | 0.352 | -0.272 | -0.493 | 0.150 | good | good | bad | **N** |
| MPI-ESM1-2-LR | r19i1p1f1 | good | bad | 0.324 | 0.244 | 0.378 | -0.020 | -0.216 | 0.211 | reasonable | reasonable | bad | **N** |
| MPI-ESM1-2-LR | r1i1p1f1 | good | reasonable | 0.334 | 0.263 | 0.389 | -0.065 | -0.272 | 0.104 | reasonable | good | reasonable | **N** |
| MPI-ESM1-2-LR | r20i1p1f1 | good | reasonable | 0.290 | 0.234 | 0.333 | 0.081 | -0.132 | 0.286 | good | reasonable | reasonable | **N** |
| MPI-ESM1-2-LR | r21i1p1f1 | good | bad | 0.404 | 0.319 | 0.460 | -0.152 | -0.372 | 0.025 | bad | good | bad | **N** |
| MPI-ESM1-2-LR | r22i1p1f1 | good | reasonable | 0.345 | 0.266 | 0.396 | 0.096 | -0.225 | 0.388 | reasonable | reasonable | reasonable | **N** |
| MPI-ESM1-2-LR | r23i1p1f1 | good | bad | 0.314 | 0.238 | 0.360 | 0.209 | -0.143 | 0.660 | reasonable | reasonable | bad | **N** |
| MPI-ESM1-2-LR | r24i1p1f1 | good | bad | 0.340 | 0.268 | 0.384 | 0.204 | -0.044 | 0.502 | reasonable | reasonable | bad | **N** |
| MPI-ESM1-2-LR | r25i1p1f1 | reasonable | bad | 0.331 | 0.265 | 0.378 | -0.055 | -0.570 | 0.170 | reasonable | good | bad | **N** |
| MPI-ESM1-2-LR | r26i1p1f1 | good | bad | 0.343 | 0.271 | 0.409 | 0.334 | -0.022 | 0.573 | reasonable | reasonable | bad | **N** |
| MPI-ESM1-2-LR | r27i1p1f1 | reasonable | bad | 0.336 | 0.269 | 0.378 | 0.038 | -0.357 | 0.214 | reasonable | reasonable | bad | **N** |
| MPI-ESM1-2-LR | r28i1p1f1 | good | reasonable | 0.342 | 0.274 | 0.388 | 0.028 | -0.198 | 0.240 | reasonable | reasonable | reasonable | **N** |
| MPI-ESM1-2-LR | r29i1p1f1 | good | bad | 0.287 | 0.227 | 0.321 | 0.167 | -0.023 | 0.438 | good | reasonable | bad | **N** |
| MPI-ESM1-2-LR | r2i1p1f1 | good | bad | 0.222 | 0.175 | 0.268 | 0.271 | -0.072 | 0.503 | good | reasonable | bad | **N** |
| MPI-ESM1-2-LR | r30i1p1f1 | good | bad | 0.289 | 0.215 | 0.336 | 0.003 | -0.171 | 0.189 | good | reasonable | bad | **N** |
| MPI-ESM1-2-LR | r31i1p1f1 | good | reasonable | 0.266 | 0.207 | 0.305 | 0.161 | -0.026 | 0.384 | good | reasonable | reasonable | **N** |
| MPI-ESM1-2-LR | r32i1p1f1 | good | bad | 0.344 | 0.242 | 0.404 | -0.063 | -0.392 | 0.112 | reasonable | good | bad | **N** |
| MPI-ESM1-2-LR | r33i1p1f1 | good | bad | 0.275 | 0.210 | 0.321 | 0.308 | 0.085 | 0.572 | good | reasonable | bad | **N** |
| MPI-ESM1-2-LR | r34i1p1f1 | reasonable | bad | 0.343 | 0.270 | 0.398 | -0.360 | -0.621 | -0.200 | reasonable | good | bad | **N** |
| MPI-ESM1-2-LR | r35i1p1f1 | good | bad | 0.378 | 0.291 | 0.439 | 0.050 | -0.153 | 0.257 | reasonable | reasonable | bad | **N** |
| MPI-ESM1-2-LR | r36i1p1f1 | reasonable | reasonable | 0.374 | 0.286 | 0.409 | 0.083 | -0.292 | 0.742 | reasonable | reasonable | reasonable | **N** |
| MPI-ESM1-2-LR | r37i1p1f1 | reasonable | reasonable | 0.373 | 0.309 | 0.414 | -0.058 | -0.512 | 0.125 | bad | good | bad | **N** |
| MPI-ESM1-2-LR | r38i1p1f1 | good | bad | 0.246 | 0.196 | 0.282 | 0.214 | -0.012 | 0.444 | good | reasonable | bad | **N** |
| MPI-ESM1-2-LR | r39i1p1f1 | reasonable | bad | 0.279 | 0.226 | 0.317 | 0.013 | -0.192 | 0.245 | good | reasonable | bad | **N** |
| MPI-ESM1-2-LR | r3i1p1f1 | reasonable | reasonable | 0.327 | 0.260 | 0.362 | -0.023 | -0.223 | 0.267 | reasonable | reasonable | reasonable | **N** |
| MPI-ESM1-2-LR | r40i1p1f1 | good | good | 0.247 | 0.193 | 0.285 | -0.120 | -0.302 | 0.041 | good | good | good | **Y** |
| MPI-ESM1-2-LR | r41i1p1f1 | reasonable | reasonable | 0.309 | 0.228 | 0.353 | 0.176 | -0.049 | 0.463 | reasonable | reasonable | reasonable | **N** |
| MPI-ESM1-2-LR | r42i1p1f1 | reasonable | bad | 0.287 | 0.219 | 0.347 | 0.320 | -0.126 | 0.663 | good | reasonable | bad | **N** |
| MPI-ESM1-2-LR | r43i1p1f1 | reasonable | reasonable | 0.306 | 0.226 | 0.351 | 0.069 | -0.269 | 0.459 | reasonable | reasonable | reasonable | **N** |
| MPI-ESM1-2-LR | r44i1p1f1 | reasonable | good | 0.332 | 0.264 | 0.382 | 0.122 | -0.165 | 0.363 | reasonable | reasonable | reasonable | **N** |
| MPI-ESM1-2-LR | r45i1p1f1 | good | bad | 0.332 | 0.249 | 0.377 | 0.170 | -0.069 | 0.454 | reasonable | reasonable | bad | **N** |
| MPI-ESM1-2-LR | r46i1p1f1 | good | bad | 0.373 | 0.280 | 0.427 | 0.155 | -0.017 | 0.359 | reasonable | reasonable | bad | **N** |

| | | | | | | | | | | | | | |
|---|---|---|---|---|---|---|---|---|---|---|---|---|---|
| MPI-ESM1-2-LR | r47i1p1f1 | reasonable | bad | 0.318 | 0.246 | 0.367 | -0.039 | -0.331 | 0.102 | reasonable | good | bad | **N** |
| MPI-ESM1-2-LR | r48i1p1f1 | reasonable | reasonable | 0.322 | 0.256 | 0.364 | 0.199 | -0.056 | 0.439 | reasonable | reasonable | reasonable | **N** |
| MPI-ESM1-2-LR | r49i1p1f1 | reasonable | bad | 0.300 | 0.244 | 0.340 | 0.162 | -0.150 | 0.394 | good | reasonable | bad | **N** |
| MPI-ESM1-2-LR | r4i1p1f1 | reasonable | bad | 0.334 | 0.233 | 0.380 | 0.189 | -0.052 | 0.741 | reasonable | reasonable | bad | **N** |
| MPI-ESM1-2-LR | r50i1p1f1 | good | reasonable | 0.256 | 0.195 | 0.297 | 0.291 | 0.062 | 0.529 | good | reasonable | reasonable | **N** |
| MPI-ESM1-2-LR | r5i1p1f1 | good | bad | 0.274 | 0.153 | 0.316 | 0.256 | 0.045 | 1.145 | good | reasonable | bad | **N** |
| MPI-ESM1-2-LR | r6i1p1f1 | reasonable | good | 0.322 | 0.259 | 0.362 | 0.164 | -0.047 | 0.418 | reasonable | reasonable | reasonable | **N** |
| MPI-ESM1-2-LR | r7i1p1f1 | good | reasonable | 0.250 | 0.192 | 0.305 | 0.206 | -0.325 | 0.506 | good | reasonable | reasonable | **N** |
| MPI-ESM1-2-LR | r8i1p1f1 | reasonable | good | 0.369 | 0.272 | 0.426 | 0.111 | -0.145 | 0.356 | reasonable | reasonable | reasonable | **N** |
| MPI-ESM1-2-LR | r9i1p1f1 | reasonable | reasonable | 0.3426114982 | 0.2475296308 | 0.3969847817 | 0.2392632176 | 0.02392924717 | 0.5608027809 | reasonable | reasonable | reasonable | **N** |
| MRI-ESM2-0 | r1i1p1f1 | good | good | 0.1857649706 | 0.1411745915 | 0.2145400145 | 0.2168548831 | -0.01187444286 | 0.5364713869 | good | reasonable | reasonable | **Y** |
| CNRM-CM6-1-HR | r1i1p1f2 | reasonable, peak increases not decreases | good | 0.1822175184 | 0.1406609306 | 0.2139286632 | -0.1487924774 | -0.4795332781 | 0.1115792905 | good | good | reasonable | **Y** |
| CNRM-CM6-1 | r1i1p1f2 | reasonable, peak increases not decreases | good | 0.165 | 0.129 | 0.193 | -0.495 | -0.831 | -0.269 | good | good | reasonable | **Y** |
| EC-Earth3P-HR | r1i1p1f1 | good | good | 0.181 | 0.168 | 0.194 | -0.202 | -0.508 | -0.179 | good | good | good | **Y** |
| EC-Earth3P-HR | r2i1p1f1 | good | good | 0.183 | 0.141 | 0.212 | -0.066 | -0.340 | 0.294 | good | good | good | **N** |
| EC-Earth3P-HR | r3i1p1f1 | good | good | 0.205 | 0.165 | 0.232 | 0.009 | -0.630 | 0.169 | good | reasonable | reasonable | **N** |
| EC-Earth3P | r1i1p1f1 | good | good | 0.186 | 0.175 | 0.195 | -0.382 | -0.457 | -0.310 | good | good | good | **Y** |
| EC-Earth3P | r2i1p1f1 | good | good | 0.198 | 0.161 | 0.223 | -0.097 | -0.281 | 0.072 | good | good | good | **N** |
| EC-Earth3P | r3i1p1f1 | good | good | 0.190 | 0.140 | 0.217 | 0.020 | -0.153 | 0.230 | good | reasonable | reasonable | **N** |
| HadGEM3-GC31-HM | r1i1p1f1 | reasonable, peak increases not decreases | good | 0.205 | 0.170 | 0.231 | -0.106 | -0.296 | 0.074 | good | good | reasonable | **Y** |
| HadGEM3-GC31-HM | r1i2p1f1 | reasonable, peak increases not decreases | good | 0.174 | 0.142 | 0.201 | -0.121 | -0.563 | 0.110 | good | good | reasonable | **N** |
| HadGEM3-GC31-HM | r1i3p1f1 | reasonable, peak increases not decreases | good | 0.202 | 0.162 | 0.237 | -0.075 | -0.349 | 0.130 | good | good | reasonable | **N** |
| HadGEM3-GC31-LM | r1i1p1f1 | reasonable, summer a little flat | good | 0.179 | 0.138 | 0.206 | -0.046 | -0.255 | 0.154 | good | good | reasonable | **Y** |

| | | | | | | | | | | | | | |
|---|---|---|---|---|---|---|---|---|---|---|---|---|---|
| HadGEM3-GC31-MM | r1i1p1f1 | reasonable, summer a little flat | good | 0.151040039 | 0.108216857 | 0.1757342771 | 0.09890227433 | -0.2201794102 | 0.4591785786 | reasonable | reasonable | reasonable | Y |
| HadGEM3-GC31-MM | r1i2p1f1 | reasonable, summer a little flat | good | 0.2109031524 | 0.1746975048 | 0.2383760621 | -0.3504469311 | -0.5976648015 | -0.1128278283 | good | good | reasonable | N |
| HadGEM3-GC31-MM | r1i3p1f1 | reasonable, summer a little flat | good | 0.1849322386 | 0.1431420447 | 0.2150640146 | 0.1890342515 | -0.02360962646 | 0.4358128719 | good | reasonable | reasonable | N |

**Table S3: Model evaluation for FWI95 – Northwest Iberia.** Evaluation results of the climate models considered for attribution analysis of FWI95 in the Northwest Iberia region. For each model, the best estimates of the Scale and Shape parameters of the GEV are shown, along with 95% confidence intervals. If the best estimate of these parameters falls within the 95% CI for the reanalysis, the model was evaluated as good; else if the 95% CIs of the model and reanalysis overlapped it was rated as reasonable; and otherwise was rated as a bad representation of the extreme FWI95 distribution. Furthermore evaluation of the seasonal cycle and spatial pattern are shown, which were evaluated by visual comparison of the seasonal and geospatial climatology to reanalysis patterns – comparison figures available on zenodo. The lowest realisation member of each model with all “good” ratings was included in the final analysis, if there was no realisation meeting that criteria, the lowest overall “reasonable” model was included.

| | | | | Sigma parameter Obs Min: 0.0734 Obs Max: 0.142 | | | Shape parameter Obs Min: -0.890 Obs Max: -0.269 | | | | | | |
|---|---|---|---|---|---|---|---|---|---|---|---|---|---|
| Model | Member | Seasonal cycle | Spatial pattern | Best estimate | Lower bound | Upper bound | Best estimate | Lower bound | Upper bound | Sigma | Shape | Rating | Model Inclusion |
| AWI-ESM-1-REcoM | r1i1p1f1 | good | reasonable | 0.124 | 0.090 | 0.151 | -0.307 | -0.626 | -0.069 | reasonable | good | reasonable | **Y** |
| CanESM5 | r1i1p2f1 | good | bad | 0.156 | 0.120 | 0.186 | -0.565 | -0.765 | -0.384 | bad | good | bad | **N** |
| CanESM5 | r8i1p1f1 | good | bad | 0.111 | 0.081 | 0.135 | -0.327 | -0.654 | -0.054 | reasonable | good | bad | **N** |
| CNRM-CM6-1-HR | r1i1p1f2 | good | good | 0.204 | 0.155 | 0.243 | -0.545 | -0.781 | -0.324 | bad | good | bad | **N** |
| CNRM-CM6-1 | r1i1p1f2 | good | reasonable | 0.154 | 0.119 | 0.176 | -0.534 | -0.732 | -0.339 | bad | good | bad | **N** |
| CNRM-ESM2-1 | r1i1p1f2 | good | reasonable | 0.145 | 0.110 | 0.175 | -0.492 | -0.746 | -0.387 | bad | good | bad | **Y** |
| GFDL-CM4 | r1i1p1f1 | good | good | 0.274 | 0.202 | 0.341 | -0.634 | -0.872 | -0.427 | bad | bad | bad | **N** |
| INM-CM4-8 | r1i1p1f1 | good | reasonable | 0.071 | 0.057 | 0.082 | -0.408 | -0.570 | -0.273 | good | good | reasonable | **Y** |
| INM-CM5-0 | r1i1p1f1 | good | reasonable | 0.089 | 0.058 | 0.109 | -0.356 | -0.625 | -0.039 | good | good | reasonable | **Y** |
| MIROC6 | r1i1p1f1 | good | reasonable | 0.102 | 0.082 | 0.120 | -0.445 | -0.697 | -0.335 | good | good | reasonable | **Y** |
| MIROC6 | r2i1p1f1 | good | reasonable | 0.117 | 0.085 | 0.136 | -0.232 | -0.443 | 0.059 | reasonable | good | reasonable | **N** |
| MIROC6 | r3i1p1f1 | good | reasonable | 0.137 | 0.081 | 0.176 | -0.344 | -0.642 | -0.041 | reasonable | good | reasonable | **N** |
| MPI-ESM1-2-LR | r10i1p1f1 | good | reasonable | 0.149 | 0.124 | 0.169 | -0.083 | -0.383 | 0.108 | bad | good | bad | **N** |
| MPI-ESM1-2-LR | r11i1p1f1 | good | reasonable | 0.155 | 0.112 | 0.184 | 0.010 | -0.217 | 0.342 | bad | reasonable | bad | **N** |
| MPI-ESM1-2-LR | r12i1p1f1 | good | reasonable | 0.159 | 0.125 | 0.181 | -0.079 | -0.247 | 0.186 | bad | good | bad | **N** |
| MPI-ESM1-2-LR | r13i1p1f1 | good | reasonable | 0.141 | 0.101 | 0.162 | -0.075 | -0.229 | 0.166 | reasonable | good | reasonable | **N** |

| | | | | | | | | | | | | | |
|---|---|---|---|---|---|---|---|---|---|---|---|---|---|
| MPI-ESM1-2-LR | r14i1p1f1 | good | reasonable | 0.147 | 0.110 | 0.175 | -0.148 | -0.488 | 0.048 | bad | good | bad | **N** |
| MPI-ESM1-2-LR | r16i1p1f1 | good | reasonable | 0.167 | 0.134 | 0.188 | -0.173 | -0.343 | 0.046 | bad | good | bad | **N** |
| MPI-ESM1-2-LR | r17i1p1f1 | good | reasonable | 0.165 | 0.129 | 0.187 | -0.012 | -0.285 | 0.300 | bad | reasonable | bad | **N** |
| MPI-ESM1-2-LR | r19i1p1f1 | good | reasonable | 0.138 | 0.105 | 0.161 | -0.251 | -0.466 | -0.046 | reasonable | good | reasonable | **N** |
| MPI-ESM1-2-LR | r1i1p1f1 | good | reasonable | 0.172 | 0.133 | 0.205 | -0.374 | -0.760 | -0.243 | bad | good | bad | **Y** |
| MPI-ESM1-2-LR | r20i1p1f1 | good | reasonable | 0.157 | 0.124 | 0.181 | -0.122 | -0.334 | 0.108 | bad | good | bad | **N** |
| MPI-ESM1-2-LR | r22i1p1f1 | good | reasonable | 0.181 | 0.136 | 0.210 | -0.170 | -0.376 | 0.008 | bad | good | bad | **N** |
| MPI-ESM1-2-LR | r23i1p1f1 | good | reasonable | 0.208 | 0.151 | 0.252 | -0.157 | -0.690 | 0.171 | bad | good | bad | **N** |
| MPI-ESM1-2-LR | r24i1p1f1 | good | reasonable | 0.135 | 0.109 | 0.157 | -0.112 | -0.308 | 0.106 | reasonable | good | reasonable | **N** |
| MPI-ESM1-2-LR | r25i1p1f1 | good | reasonable | 0.170 | 0.135 | 0.198 | -0.112 | -0.502 | 0.087 | bad | good | bad | **N** |
| MPI-ESM1-2-LR | r26i1p1f1 | good | reasonable | 0.167 | 0.119 | 0.198 | -0.281 | -0.688 | 0.048 | bad | good | bad | **N** |
| MPI-ESM1-2-LR | r27i1p1f1 | good | reasonable | 0.181 | 0.137 | 0.217 | -0.394 | -0.663 | -0.162 | bad | good | bad | **N** |
| MPI-ESM1-2-LR | r28i1p1f1 | good | reasonable | 0.227 | 0.182 | 0.265 | -0.255 | -0.610 | -0.070 | bad | good | bad | **N** |
| MPI-ESM1-2-LR | r29i1p1f1 | good | reasonable | 0.170 | 0.141 | 0.193 | -0.272 | -0.652 | -0.110 | bad | good | bad | **N** |
| MPI-ESM1-2-LR | r2i1p1f1 | good | reasonable | 0.197 | 0.150 | 0.233 | -0.217 | -0.625 | 0.007 | bad | good | bad | **N** |
| MPI-ESM1-2-LR | r30i1p1f1 | good | reasonable | 0.126 | 0.092 | 0.147 | 0.136 | -0.061 | 0.493 | reasonable | reasonable | reasonable | **N** |
| MPI-ESM1-2-LR | r32i1p1f1 | good | reasonable | 0.152 | 0.126 | 0.172 | -0.208 | -0.477 | -0.041 | bad | good | bad | **N** |
| MPI-ESM1-2-LR | r33i1p1f1 | good | reasonable | 0.164 | 0.132 | 0.185 | -0.121 | -0.345 | 0.070 | bad | good | bad | **N** |
| MPI-ESM1-2-LR | r34i1p1f1 | good | reasonable | 0.188 | 0.152 | 0.224 | -0.151 | -0.480 | 0.061 | bad | good | bad | **N** |
| MPI-ESM1-2-LR | r35i1p1f1 | good | reasonable | 0.155 | 0.115 | 0.179 | 0.069 | -0.087 | 0.332 | bad | reasonable | bad | **N** |
| MPI-ESM1-2-LR | r36i1p1f1 | good | reasonable | 0.180 | 0.148 | 0.206 | -0.153 | -0.365 | -0.013 | bad | good | bad | **N** |
| MPI-ESM1-2-LR | r37i1p1f1 | good | reasonable | 0.164 | 0.125 | 0.192 | -0.310 | -0.514 | -0.149 | bad | good | bad | **N** |
| MPI-ESM1-2-LR | r38i1p1f1 | good | reasonable | 0.174 | 0.143 | 0.201 | -0.356 | -0.748 | -0.210 | bad | good | bad | **N** |
| MPI-ESM1-2-LR | r39i1p1f1 | good | reasonable | 0.167 | 0.122 | 0.192 | -0.027 | -0.260 | 0.337 | bad | reasonable | bad | **N** |
| MPI-ESM1-2-LR | r3i1p1f1 | good | reasonable | 0.137 | 0.102 | 0.169 | 0.064 | -0.301 | 0.411 | reasonable | reasonable | reasonable | **N** |
| MPI-ESM1-2-LR | r40i1p1f1 | good | reasonable | 0.182 | 0.137 | 0.216 | -0.071 | -0.398 | 0.308 | bad | good | bad | **N** |
| MPI-ESM1-2-LR | r41i1p1f1 | good | reasonable | 0.151 | 0.110 | 0.183 | -0.030 | -0.400 | 0.308 | bad | reasonable | bad | **N** |
| MPI-ESM1-2-LR | r42i1p1f1 | good | reasonable | 0.154 | 0.099 | 0.185 | 0.018 | -0.206 | 0.580 | reasonable | reasonable | reasonable | **N** |
| MPI-ESM1-2-LR | r43i1p1f1 | good | reasonable | 0.179 | 0.126 | 0.209 | -0.117 | -0.318 | 0.165 | bad | good | bad | **N** |
| MPI-ESM1-2-LR | r44i1p1f1 | good | reasonable | 0.166 | 0.125 | 0.192 | 0.070 | -0.099 | 0.285 | bad | reasonable | bad | **N** |
| MPI-ESM1-2-LR | r45i1p1f1 | good | reasonable | 0.192 | 0.145 | 0.222 | -0.192 | -0.387 | -0.034 | bad | good | bad | **N** |
| MPI-ESM1-2-LR | r46i1p1f1 | good | reasonable | 0.164 | 0.122 | 0.192 | -0.209 | -0.422 | 0.024 | bad | good | bad | **N** |
| MPI-ESM1-2-LR | r47i1p1f1 | good | reasonable | 0.197 | 0.153 | 0.229 | -0.159 | -0.456 | 0.028 | bad | good | bad | **N** |
| MPI-ESM1-2-LR | r48i1p1f1 | good | reasonable | 0.147 | 0.109 | 0.171 | -0.297 | -0.462 | -0.044 | reasonable | good | reasonable | **N** |

| | | | | | | | | | | | | | |
|---|---|---|---|---|---|---|---|---|---|---|---|---|---|
| MPI-ESM1-2-LR | r49i1p1f1 | good | reasonable | 0.170 | 0.132 | 0.199 | -0.455 | -0.668 | -0.288 | bad | good | bad | **N** |
| MPI-ESM1-2-LR | r4i1p1f1 | good | reasonable | 0.121 | 0.082 | 0.151 | 0.221 | -0.167 | 0.696 | reasonable | reasonable | reasonable | **N** |
| MPI-ESM1-2-LR | r50i1p1f1 | good | reasonable | 0.180 | 0.143 | 0.210 | -0.330 | -0.574 | -0.188 | bad | good | bad | **N** |
| MPI-ESM1-2-LR | r5i1p1f1 | good | reasonable | 0.161 | 0.126 | 0.186 | -0.212 | -0.415 | -0.028 | bad | good | bad | **N** |
| MPI-ESM1-2-LR | r6i1p1f1 | good | reasonable | 0.181 | 0.128 | 0.228 | -0.189 | -0.661 | 0.125 | bad | good | bad | **N** |
| MPI-ESM1-2-LR | r7i1p1f1 | good | reasonable | 0.190 | 0.152 | 0.216 | -0.146 | -0.416 | 0.173 | bad | good | bad | **N** |
| MPI-ESM1-2-LR | r8i1p1f1 | good | reasonable | 0.169 | 0.136 | 0.196 | -0.360 | -0.667 | -0.105 | bad | good | bad | **N** |
| MPI-ESM1-2-LR | r9i1p1f1 | good | reasonable | 0.167 | 0.136 | 0.189 | -0.141 | -0.456 | 0.069 | bad | good | bad | **N** |
| MRI-ESM2-0 | r1i1p1f1 | good | good | 0.215 | 0.156 | 0.261 | 0.126 | -0.115 | 0.428 | bad | reasonable | bad | **N** |
| CNRM-CM6-1-HR | r1i1p1f2 | good | good | 0.091 | 0.064 | 0.110 | -0.636 | -0.849 | -0.428 | good | bad | bad | **Y** |
| CNRM-CM6-1 | r1i1p1f2 | good | reasonable | 0.081 | 0.063 | 0.094 | -0.388 | -0.565 | -0.262 | good | good | reasonable | **Y** |
| EC-Earth3P-HR | r1i1p1f1 | good | good | 0.08674464903 | 0.0814641846 | 0.091249559 | -0.08541416759 | -0.13774235133 | -0.03706593499 | good | good | good | **N** |
| EC-Earth3P-HR | r2i1p1f1 | good | good | 0.0793610298 | 0.05644659109 | 0.09501150459 | -0.09110816072 | -0.323599439 | 0.1313193189 | good | good | good | **Y** |
| EC-Earth3P-HR | r3i1p1f1 | good | good | 0.0586299077 | 0.04771162107 | 0.0684618968 | -0.4086354994 | -0.8083095445 | -0.2862209641 | good | good | good | **N** |
| EC-Earth3P | r1i1p1f1 | good | good | 0.091 | 0.064 | 0.110 | -0.636 | -0.849 | -0.428 | good | bad | bad | **Y** |
| EC-Earth3P | r2i1p1f1 | good | good | 0.064 | 0.051 | 0.073 | -0.142 | -0.324 | 0.092 | good | good | good | **N** |
| EC-Earth3P | r3i1p1f1 | good | good | 0.076 | 0.057 | 0.087 | -0.329 | -0.603 | -0.151 | good | good | good | **N** |
| HadGEM3-GC31-HM | r1i1p1f1 | good | good | 0.071 | 0.052 | 0.081 | -0.133 | -0.337 | 0.096 | good | good | good | **Y** |
| HadGEM3-GC31-HM | r1i2p1f1 | good | good | 0.073 | 0.056 | 0.085 | -0.423 | -0.792 | -0.157 | good | good | good | **N** |
| HadGEM3-GC31-HM | r1i3p1f1 | good | good | 0.070 | 0.057 | 0.082 | -0.174 | -0.390 | -0.031 | good | good | good | **N** |
| HadGEM3-GC31-LM | r1i1p1f1 | good | reasonable | 0.087 | 0.065 | 0.099 | -0.239 | -0.424 | 0.037 | good | good | reasonable | **N** |
| HadGEM3-GC31-MM | r1i1p1f1 | good | good | 0.085 | 0.049 | 0.106 | -0.264 | -0.485 | 0.109 | good | good | good | **N** |
| HadGEM3-GC31-MM | r1i2p1f1 | good | good | 0.075 | 0.057 | 0.089 | -0.347 | -0.628 | -0.168 | good | good | good | **Y** |
| HadGEM3-GC31-MM | r1i3p1f1 | good | good | 0.100 | 0.082 | 0.114 | -0.251 | -0.520 | -0.111 | good | good | good | **N** |

**Table S4: Model evaluation for FWI95 – Chilean Temperate Forest and Matorral.** Evaluation results of the climate models considered for attribution analysis of FWI95 in the Chilean Temperate Forest and Matorral region. For each model, the best estimates of the Scale and Shape parameters of the GEV are shown, along with 95% confidence intervals. If the best estimate of these parameters falls within the 95% CI for the reanalysis, the model was evaluated as good; else if the 95% CIs of the model and reanalysis overlapped it was rated as reasonable; and otherwise was rated as a bad representation of the extreme FWI95 distribution. Furthermore evaluation of the seasonal cycle and spatial pattern are shown, which were evaluated by visual comparison of the seasonal and geospatial climatology to reanalysis patterns – comparison figures available on zenodo. The lowest realisation member of each model with all “good” ratings was included in the final analysis, if there was no realisation meeting that criteria, the lowest overall “reasonable” model was included.

| | | | | **Sigma parameter Obs Min: 0.0734 Obs Max: 0.142** | | | **Shape parameter Obs Min: -0.890 Obs Max: -0.269** | | | | | | |
|---|---|---|---|---|---|---|---|---|---|---|---|---|---|
| **Model** | **Member** | **Seasonal cycle** | **Spatial pattern** | Best estimate | Lower bound | Upper bound | Best estimate | Lower bound | Upper bound | **Sigma** | **Shape** | **Rating** | **Model Inclusion** |
| AWI-ESM-1-REcoM | r1i1p1f1 | good | reasonable | 0.054 | 0.042 | 0.061 | -0.612 | -0.865 | -0.267 | reasonable | good | reasonable | **Y** |
| CanESM5 | r1i1p2f1 | good | reasonable | 0.051 | 0.037 | 0.061 | -0.352 | -0.706 | -0.132 | bad | good | bad | **Y** |
| CanESM5 | r8i1p1f1 | good | reasonable | 0.068 | 0.053 | 0.081 | -0.430 | -0.719 | -0.279 | good | good | reasonable | **N** |
| CNRM-CM6-1-HR | r1i1p1f2 | good | good | 0.077 | 0.063 | 0.088 | -0.661 | -0.891 | -0.441 | good | good | good | **N** |
| CNRM-CM6-1 | r1i1p1f2 | good | reasonable | 0.061 | 0.051 | 0.068 | -0.362 | -0.654 | -0.264 | reasonable | good | reasonable | **N** |
| CNRM-ESM2-1 | r1i1p1f2 | good | reasonable | 0.070 | 0.049 | 0.086 | -0.413 | -0.724 | -0.208 | good | good | reasonable | **Y** |
| GFDL-CM4 | r1i1p1f1 | good | reasonable | 0.081 | 0.062 | 0.098 | -0.569 | -0.839 | -0.410 | good | good | reasonable | **Y** |
| INM-CM4-8 | r1i1p1f1 | good | bad, central south too firey | 0.051 | 0.040 | 0.058 | -0.194 | -0.480 | -0.032 | bad | bad | bad | **N** |
| INM-CM5-0 | r1i1p1f1 | good | bad, central south too firey | 0.055 | 0.042 | 0.063 | -0.240 | -0.551 | 0.041 | reasonable | bad | bad | **N** |
| MIROC6 | r1i1p1f1 | good | reasonable | 0.056 | 0.044 | 0.067 | -0.717 | -0.926 | -0.547 | reasonable | good | reasonable | **N** |
| MIROC6 | r2i1p1f1 | good | reasonable | 0.087 | 0.061 | 0.104 | -0.572 | -0.765 | -0.350 | good | good | reasonable | **Y** |
| MIROC6 | r3i1p1f1 | good | reasonable | 0.061 | 0.046 | 0.073 | -0.428 | -0.688 | -0.287 | good | good | reasonable | **N** |
| MPI-ESM1-2-LR | r10i1p1f1 | good | reasonable | 0.061 | 0.048 | 0.071 | -0.378 | -0.600 | -0.177 | good | good | reasonable | **N** |
| MPI-ESM1-2-LR | r11i1p1f1 | good | reasonable | 0.039 | 0.031 | 0.045 | -0.192 | -0.484 | -0.052 | bad | bad | bad | **N** |
| MPI-ESM1-2-LR | r12i1p1f1 | good | reasonable | 0.061 | 0.045 | 0.072 | -0.431 | -0.653 | -0.278 | good | good | reasonable | **N** |
| MPI-ESM1-2-LR | r13i1p1f1 | good | reasonable | 0.051 | 0.036 | 0.062 | -0.366 | -0.645 | -0.191 | reasonable | good | reasonable | **N** |
| MPI-ESM1-2-LR | r14i1p1f1 | good | reasonable | 0.047 | 0.038 | 0.053 | -0.243 | -0.525 | -0.100 | bad | bad | bad | **N** |
| MPI-ESM1-2-LR | r15i1p1f1 | good | reasonable | 0.053 | 0.039 | 0.064 | -0.438 | -0.685 | -0.263 | reasonable | good | reasonable | **N** |
| MPI-ESM1-2-LR | r16i1p1f1 | good | reasonable | 0.043 | 0.034 | 0.051 | -0.528 | -0.798 | -0.378 | bad | good | bad | **N** |
| MPI-ESM1-2-LR | r17i1p1f1 | good | reasonable | 0.059 | 0.044 | 0.070 | -0.487 | -0.775 | -0.214 | reasonable | good | reasonable | **N** |
| MPI-ESM1-2-LR | r18i1p1f1 | good | reasonable | 0.065 | 0.051 | 0.078 | -0.627 | -0.878 | -0.455 | good | good | reasonable | **N** |
| MPI-ESM1-2-LR | r19i1p1f1 | good | reasonable | 0.065 | 0.043 | 0.078 | -0.461 | -0.667 | -0.222 | good | good | reasonable | **N** |
| MPI-ESM1-2-LR | r1i1p1f1 | good | reasonable | 0.053 | 0.040 | 0.063 | -0.363 | -0.673 | -0.252 | reasonable | good | reasonable | **Y** |
| MPI-ESM1-2-LR | r20i1p1f1 | good | reasonable | 0.050 | 0.040 | 0.058 | -0.186 | -0.345 | -0.038 | bad | bad | bad | **N** |
| MPI-ESM1-2-LR | r21i1p1f1 | good | reasonable | 0.053 | 0.042 | 0.063 | -0.180 | -0.411 | 0.003 | reasonable | bad | bad | **N** |
| MPI-ESM1-2-LR | r22i1p1f1 | good | reasonable | 0.057 | 0.036 | 0.069 | -0.366 | -0.590 | -0.070 | reasonable | good | reasonable | **N** |
| MPI-ESM1-2-LR | r23i1p1f1 | good | reasonable | 0.063 | 0.049 | 0.073 | -0.373 | -0.578 | -0.212 | good | good | reasonable | **N** |

| | | | | | | | | | | | | | |
|---|---|---|---|---|---|---|---|---|---|---|---|---|---|
| MPI-ESM1-2-LR | r24i1p1f1 | good | reasonable | 0.057 | 0.044 | 0.067 | -0.505 | -0.742 | -0.289 | reasonable | good | reasonable | **N** |
| MPI-ESM1-2-LR | r25i1p1f1 | good | reasonable | 0.050 | 0.040 | 0.059 | -0.281 | -0.608 | -0.028 | bad | bad | bad | **N** |
| MPI-ESM1-2-LR | r26i1p1f1 | good | reasonable | 0.046 | 0.036 | 0.053 | -0.248 | -0.443 | -0.090 | bad | bad | bad | **N** |
| MPI-ESM1-2-LR | r27i1p1f1 | good | reasonable | 0.049 | 0.031 | 0.059 | -0.278 | -0.566 | 0.303 | bad | reasonable | bad | **N** |
| MPI-ESM1-2-LR | r28i1p1f1 | good | reasonable | 0.042 | 0.034 | 0.048 | -0.187 | -0.360 | -0.032 | bad | bad | bad | **N** |
| MPI-ESM1-2-LR | r29i1p1f1 | good | reasonable | 0.067 | 0.055 | 0.077 | -0.496 | -0.718 | -0.313 | good | good | reasonable | **N** |
| MPI-ESM1-2-LR | r2i1p1f1 | good | reasonable | 0.048 | 0.032 | 0.060 | -0.662 | -0.875 | -0.354 | bad | good | bad | **N** |
| MPI-ESM1-2-LR | r30i1p1f1 | good | reasonable | 0.049 | 0.040 | 0.057 | -0.424 | -0.703 | -0.295 | bad | good | bad | **N** |
| MPI-ESM1-2-LR | r31i1p1f1 | good | reasonable | 0.044 | 0.033 | 0.053 | -0.257 | -0.544 | -0.031 | bad | bad | bad | **N** |
| MPI-ESM1-2-LR | r32i1p1f1 | good | reasonable | 0.046 | 0.035 | 0.054 | -0.237 | -0.436 | -0.044 | bad | bad | bad | **N** |
| MPI-ESM1-2-LR | r33i1p1f1 | good | reasonable | 0.057 | 0.043 | 0.067 | -0.336 | -0.507 | -0.152 | reasonable | bad | bad | **N** |
| MPI-ESM1-2-LR | r34i1p1f1 | good | reasonable | 0.038 | 0.026 | 0.051 | -0.231 | -0.775 | 0.189 | bad | reasonable | bad | **N** |
| MPI-ESM1-2-LR | r35i1p1f1 | good | reasonable | 0.053 | 0.038 | 0.064 | -0.315 | -0.568 | -0.063 | reasonable | bad | bad | **N** |
| MPI-ESM1-2-LR | r36i1p1f1 | good | reasonable | 0.054 | 0.043 | 0.063 | -0.359 | -0.645 | -0.220 | reasonable | good | reasonable | **N** |
| MPI-ESM1-2-LR | r37i1p1f1 | good | reasonable | 0.063 | 0.050 | 0.076 | -0.420 | -0.712 | -0.249 | good | good | reasonable | **N** |
| MPI-ESM1-2-LR | r38i1p1f1 | good | reasonable | 0.051 | 0.039 | 0.061 | -0.621 | -0.872 | -0.404 | reasonable | good | reasonable | **N** |
| MPI-ESM1-2-LR | r39i1p1f1 | good | reasonable | 0.047 | 0.038 | 0.054 | -0.145 | -0.449 | 0.008 | bad | bad | bad | **N** |
| MPI-ESM1-2-LR | r3i1p1f1 | good | reasonable | 0.048 | 0.038 | 0.056 | -0.534 | -0.805 | -0.330 | bad | good | bad | **N** |
| MPI-ESM1-2-LR | r40i1p1f1 | good | reasonable | 0.058 | 0.045 | 0.066 | -0.668 | -0.897 | -0.319 | reasonable | good | reasonable | **N** |
| MPI-ESM1-2-LR | r41i1p1f1 | good | reasonable | 0.048 | 0.034 | 0.058 | -0.426 | -0.775 | -0.081 | bad | good | bad | **N** |
| MPI-ESM1-2-LR | r42i1p1f1 | good | reasonable | 0.049 | 0.039 | 0.059 | -0.443 | -0.777 | -0.231 | bad | good | bad | **N** |
| MPI-ESM1-2-LR | r43i1p1f1 | good | reasonable | 0.046 | 0.038 | 0.053 | -0.385 | -0.676 | -0.148 | bad | good | bad | **N** |
| MPI-ESM1-2-LR | r44i1p1f1 | good | reasonable | 0.042 | 0.030 | 0.050 | -0.151 | -0.469 | 0.061 | bad | reasonable | bad | **N** |
| MPI-ESM1-2-LR | r45i1p1f1 | good | reasonable | 0.046 | 0.036 | 0.056 | -0.239 | -0.598 | -0.037 | bad | bad | bad | **N** |
| MPI-ESM1-2-LR | r46i1p1f1 | good | reasonable | 0.046 | 0.036 | 0.052 | -0.341 | -0.591 | -0.064 | bad | bad | bad | **N** |
| MPI-ESM1-2-LR | r47i1p1f1 | good | reasonable | 0.046 | 0.034 | 0.055 | -0.223 | -0.396 | -0.016 | bad | bad | bad | **N** |
| MPI-ESM1-2-LR | r48i1p1f1 | good | reasonable | 0.057 | 0.043 | 0.065 | -0.551 | -0.758 | -0.238 | reasonable | good | reasonable | **N** |
| MPI-ESM1-2-LR | r49i1p1f1 | good | reasonable | 0.061 | 0.047 | 0.073 | -0.492 | -0.793 | -0.336 | good | good | reasonable | **N** |
| MPI-ESM1-2-LR | r4i1p1f1 | good | reasonable | 0.041 | 0.033 | 0.047 | -0.197 | -0.391 | -0.025 | bad | bad | bad | **N** |
| MPI-ESM1-2-LR | r50i1p1f1 | good | reasonable | 0.058 | 0.047 | 0.067 | -0.498 | -0.767 | -0.293 | reasonable | good | reasonable | **N** |
| MPI-ESM1-2-LR | r5i1p1f1 | good | reasonable | 0.057 | 0.045 | 0.067 | -0.677 | -0.867 | -0.447 | reasonable | good | reasonable | **N** |
| MPI-ESM1-2-LR | r6i1p1f1 | good | reasonable | 0.052 | 0.039 | 0.062 | -0.472 | -0.731 | -0.315 | reasonable | good | reasonable | **N** |
| MPI-ESM1-2-LR | r7i1p1f1 | good | reasonable | 0.053 | 0.042 | 0.062 | -0.616 | -0.862 | -0.336 | reasonable | good | reasonable | **N** |
| MPI-ESM1-2-LR | r8i1p1f1 | good | reasonable | 0.055 | 0.043 | 0.064 | -0.365 | -0.600 | -0.212 | reasonable | good | reasonable | **N** |

| | | | | | | | | | | | | | |
|---|---|---|---|---|---|---|---|---|---|---|---|---|---|
| MPI-ESM1-2-LR | r9i1p1f1 | good | reasonable | 0.04586330903 | 0.03563839521 | 0.05365611964 | -0.3448855468 | -0.6916536837 | -0.1912389164 | bad | bad | bad | **N** |
| MRI-ESM2-0 | r1i1p1f1 | good | reasonable | 0.1086095373 | 0.08675606376 | 0.1262320384 | -0.5781168461 | -0.8332111742 | -0.378364324 | reasonable | good | reasonable | **Y** |
| CNRM-CM6-1-HR | r1i1p1f2 | good | good | 0.07168843287 | 0.05610196835 | 0.08282993499 | -0.6990054566 | -0.92501074 | -0.4222299845 | good | good | good | **N** |
| CNRM-CM6-1 | r1i1p1f2 | good | reasonable | 0.070 | 0.046 | 0.088 | -0.466 | -0.662 | -0.131 | good | good | reasonable | **Y** |
| EC-Earth3P-HR | r1i1p1f1 | good | good | 0.058 | 0.055 | 0.061 | -0.342 | -0.389 | -0.299 | bad | bad | bad | **N** |
| EC-Earth3P-HR | r2i1p1f1 | good | good | 0.066 | 0.046 | 0.081 | -0.327 | -0.615 | -0.102 | good | bad | bad | **Y** |
| EC-Earth3P-HR | r3i1p1f1 | good | good | 0.059 | 0.046 | 0.069 | -0.181 | -0.337 | -0.005 | reasonable | bad | bad | **N** |
| EC-Earth3P | r1i1p1f1 | good | good | 0.062 | 0.059 | 0.065 | -0.334 | -0.379 | -0.288 | good | bad | bad | **Y** |
| EC-Earth3P | r2i1p1f1 | good | good | 0.059 | 0.047 | 0.068 | -0.315 | -0.479 | -0.161 | reasonable | bad | bad | **N** |
| EC-Earth3P | r3i1p1f1 | good | good | 0.058 | 0.042 | 0.069 | -0.421 | -0.727 | -0.078 | reasonable | good | reasonable | **N** |
| HadGEM3-GC31-HM | r1i1p1f1 | good | good | 0.048 | 0.036 | 0.056 | -0.511 | -0.747 | -0.283 | bad | good | bad | **N** |
| HadGEM3-GC31-HM | r1i2p1f1 | good | good | 0.049 | 0.040 | 0.057 | -0.289 | -0.653 | -0.174 | bad | bad | bad | **N** |
| HadGEM3-GC31-HM | r1i3p1f1 | good | good | 0.057 | 0.038 | 0.069 | -0.481 | -0.706 | -0.183 | reasonable | good | reasonable | **Y** |
| HadGEM3-GC31-LM | r1i1p1f1 | good | bad | 0.044 | 0.029 | 0.052 | -0.733 | -0.954 | -0.333 | bad | good | bad | **N** |
| HadGEM3-GC31-MM | r1i1p1f1 | good | reasonable | 0.05450275773 | 0.0401268182 | 0.06536897457 | -0.5394866444 | -0.7504271674 | -0.3657179998 | reasonable | good | reasonable | **Y** |
| HadGEM3-GC31-MM | r1i2p1f1 | good | reasonable | 0.0575118544 | 0.04590591494 | 0.06888637231 | -0.5560316181 | -0.9121948922 | -0.4486011493 | reasonable | good | reasonable | **N** |
| HadGEM3-GC31-MM | r1i3p1f1 | good | reasonable | 0.05973510293 | 0.04595850706 | 0.07060338638 | -0.3456996065 | -0.5191289065 | -0.1947669175 | reasonable | bad | bad | **N** |

As described in both the 2023-24 and 2024-25 reports, a baseline period of 1960-2013 was utilised for the HadGEM3-A attribution analysis. The 2025-26 report reduces this baseline period to 1980-2013 due to the uncertainties inherent to the pre-satellite era of reanalysis products, in particular in ERA5. As stated in the final back-extension to 1940 specification; 'Trends in 2-m temperature anomalies over land for ERA5, both globally and over Europe, show generally excellent agreement with independent datasets based entirely on surface observations, particularly for the late 1970s onwards (Soci et al., 2024). Given the importance of 2-m temperature in various stages of the FWI calculation, along with poor wind field representation, the baseline period start was moved forward from 1960 to 1980. A 33 year baseline (1980-2013) is consistent with typical climatology periods of 30 years. This baseline period gives not only relevant context for the event values of FWI to past years, but is used to perform bias adjustment of the HadGEM3-A large attribution ensemble ('Attribution Ensemble'). This ensemble of 525 members is run twice, once with natural only forcings from solar variability and volcanic activity (Counterfactual) and one including anthropogenic emissions (Factual). As discussed individually in **Sections S3, S4 and S5**, the HadGEM3-A historical ensemble ('Historical Ensemble'), which is the 15-member counterpart run over the period 1960-2013 used to evaluate model performance, tends to overestimate the FWI95 value with respect to reanalysis observations in the focal regions. By applying a trend-preserving linear regression based on the historical ensemble and anchored to each year of the 2020-2024 ensemble, an effective 39,375-member attribution ensemble can be generated for both the natural and anthropogenically altered climate simulations. Bootstrapping the FWI95 value for each year 10,000 times allows for a high confidence range for the Probability Ratio to be calculated.

For the three different model analyses included in this report, slightly different variables were used for the calculation of FWI. While all use maximum daily temperature and total daily precipitation, the WWA multi-model approach uses minimum relative humidity and maximum wind speed, the HadGEM3-A large ensemble is calculated using mean relative humidity and mean wind speed, and the CMIP6 ensemble analysis uses minimum relative humidity and mean wind speed. These differences are unlikely to cause substantial changes in the results compared to the model uncertainty, but may result in larger possible ranges of PR across different metrics.

### S1.2.2. Attribution of Present Day Focal Events - BA

We follow the same overall ConFLAME framework as in the previous report. ConFLAME consists of two main components: (1) a fire model describing the controls on burned area (BA), and (2) a Bayesian inference framework used to estimate model parameters and quantify uncertainty.

1) **Fire model formulation.** The fire model represents BA as the combined effect of key controls on fire activity: fuel connectivity, fuel dryness, ignitions, and anthropogenic suppression. Each control is expressed as a linear combination of its driving variables (listed in **Table S5**), transformed using a logistic function to represent its limiting effect on burning. Each control therefore describes the maximum fraction of burned area that would occur under otherwise favourable conditions. Total BA is calculated as the product of these controls, modulated by an additional term, $Q_{spread,}$ which represents variability in fire outcomes not captured by the model drivers. This includes both unresolved processes and inherent stochasticity in fire activity.

2) **Bayesian inference and uncertainty.** Model parameters are estimated using a Maximum Entropy Bayesian inference approach. This framework identifies the range of parameter values that are consistent with observed burned area, rather than a single optimal solution. As a result, the model produces a posterior distribution of parameters, which propagates through to a distribution of modelled BA outcomes.

   $Q_{spread}$ is treated as a hierarchical parameter, meaning that it introduces additional variability conditional on the other model parameters. This allows the model to represent uncertainty arising both from parameter estimation and from unobserved variability in fire behaviour.

   The model is calibrated against MODIS burned area observations (**Sect. 2.1.2.1**). Training is conducted on a subset (10%) of the available data spanning January 2002 to February 2026, following the same inference protocol as in Kelley et al. (2025). Optimisation uses a No-U-Turns (NUTS) approach, with 1000 warm-up and 1000 sampling iterations over 10 chains. 100 samples are taken from each chain for attribution experiments.

**Table S5**: Predictors used by ConFLAME attribution setup. Drivers are grouped into four control categories. (+) or (–) signs representing positive or negative influence over fire occurrence in ConFLAME.

| *Control* | *Driver* | *Directional contribution* | *Temporal resolution* | *Factual* | *Source* | *Counterfactual* |
|---|---|---|---|---|---|---|
| **Fuel** | Tree cover | + | Snapshot 2020 | Fractional cover of Broadleaf and Needleleaf PFT | HadGEM3-A (Ciavarella et al., 2018) | ISAM-HYDE moderated by JULES V6.0 (Meiyappan, et al., 2012) |
| | Shrub cover | + | | Fractional cover of Shrub | | |
| | Herbaceous Cover | + | | Fractional cover of C3 and C4 grass | | |
| **Weather** | Maximum consecutive number of dry days | + | Monthly | Running mean of continuous days with precip < 0.1mm | ERA5 (Muñoz-Sabater et al., 2021) | ERA5 with climate change signal removed using difference between HadGEM3-A (Ciavarella et al., 2018) all forcings and natural only simulations |
| | Precipitation | – | Monthly | Monthly totals of daily precip | | |
| | Maximum monthly temperature | + | Monthly | Maximum of daily maximums for month | | |
| | Mean monthly minimum humidity | – | Monthly | Calculated as per Kelley et al. (2025) | | |
| **Ignition/ Suppression** | Pasture Fraction | + ignitions<br>- suppression | Annual | Linear interpolation to a monthly timestep | HYDE (Klein Goldewijk et al., 2010) | Kept same as factual |
| | Cropland Fraction | + ignitions<br>- suppression | Annual | | | |
| | Urban Population | - suppression | Annual | | | |
| | Rural Population | + ignitions<br>- suppression | Annual | | | |

| ***Control*** | ***Driver*** | ***Directional contribution*** | ***Temporal resolution*** | ***Factual*** | ***Source*** | ***Counterfactual*** |
|---|---|---|---|---|---|---|
| **Fuel** | Tree cover | + | Snapshot 2020 | Fractional cover of Broadleaf and Needleleaf PFT | HadGEM3-A (Ciavarella et al., 2018) | ISAM-HYDE moderated by JULES V6.0 (Meiyappan, et al., 2012) |
| | Shrub cover | + | | Fractional cover of Shrub | | |
| | Herbaceous Cover | + | | Fractional cover of C3 and C4 grass | | |
| | Cloud-to-ground lightning | + ignitions | Monthly | | (Qu et al. 2025) | |

**Attribution simulations: factual and counterfactual**
For attribution, the trained model is run in predictive mode using both factual and counterfactual inputs. The factual simulations are driven by ERA5 reanalysis data (**Table S5**) and represent the real-world meteorological conditions under which the fires occurred.

The counterfactual simulations use the same underlying ERA5 data, but with the anthropogenic climate signal removed. This is achieved using the HadGEM3-A large ensemble to estimate the difference between simulations with and without anthropogenic forcing. These differences are applied to each meteorological and fuel variable to generate counterfactual conditions consistent with a world without human influence.

This approach ensures that the timing and structure of the observed event are preserved, while isolating the effect of anthropogenic climate change. Due to the temporary unavailability of HadGEM3-A simulations beyond 2024, we use ensemble members from 2021–2024 to represent the anthropogenic signal, resulting in 2100 counterfactual realisations (4 years × 525 ensemble members).

**Ensemble generation**
We generate 1000 paired factual and counterfactual simulations by sampling from the posterior parameter distribution. For counterfactual runs, meteorological adjustments are also randomly sampled from the available HadGEM3-A ensemble members. This produces an ensemble that captures uncertainty in both model parameters and climate forcing.

In this year’s analysis, two additional constraints are introduced to improve the robustness of attribution estimates:

1. **Paired stochasticity**: Paired stochasticity: Qspread represents variability in burned area arising from factors not explicitly represented in the model, including the inherent stochasticity of fire activity. Because the aim of the attribution experiment is to isolate the influence of anthropogenic climate forcing on the observed event, we pair Qspread values between corresponding factual and counterfactual simulations. This ensures that differences between the two worlds arise from the imposed climate signal rather than random variability in fire response, analogous to the paired treatment of meteorological conditions in the factual and counterfactual forcing datasets. Stochastic variability is therefore retained within the simulations but controlled for when comparing the two worlds.
2. **Conditioning on observed burned area:** We explicitly condition the model posterior on the observed BA for the target event. This is achieved by reweighting the posterior distribution according to the likelihood of reproducing the observed BA in the factual. The likelihood term is an extension of equation 9 in Barbosa et al. (2025):

$$P\left(\beta|\left(\{BF_i\},\{X_{i,v}\} \cap \{BF_j\}\right)\right) \propto \prod_{j}^{event} P\left(\beta|\{BF_i\},\{X_{i,v}\}\right)^{BF_j} \times \left(1 - P\left(\beta|\{BF_i\},\{X_{i,v}\}\right)\right)^{1-BF_j}$$

Where $\beta$ is our parameter set, $\{BF_i\}$ is our set of historical observed burn fractions$\{X_{i,v}\}$ the driving variables, and $\{BF_j\}$ is burned area during our focal event

This weight is also applied to the paired counterfactual, and ensures that attribution focuses on the subset of model realisations consistent with the observed event. Attribution results are derived from these reweighted posterior distributions. The amplification factor (AF) is calculated as the ratio of burned area under factual and counterfactual conditions for events of equivalent likelihood, across all re-weighted posteriors (not just the portion where factual exceeded observed, as per last year).

The probability ratio (PR) is calculated as the change in likelihood of events with comparable BA between factual and counterfactual simulations.

Uncertainty ranges (5th–95th percentiles) arise directly from the posterior ensemble and reflect both parameter uncertainty and variability in fire outcomes.

### S1.2.3. Future Projections - BA

For future projections, we trained the model on ISIMIP3a GSWP3 reanalysis data and used ISIMIP3b bias-corrected GCMs to perform future projections as outlined in **Section 2.5.4**, following previous reports (Kelley et al. 2025).

ConFLAMEs uninformed priors used in previous reports included parameter combinations in which fire controls became effectively saturated. Preliminary tests this year showed that, for the smaller focal regions in this year's report, the posterior distribution did not always sufficiently constrain parts of the parameter space that implied dryness had little or no influence on burned area. This is inconsistent with the strong observational and process-based evidence that dryness conditions influence fire activity in all three focal regions (see hydroclimatic analyses in the main report). We therefore modify the update function described in Barbosa et al. (2025) by excluding parameter combinations for which the dryness control can alter the relative burned area by less than 1%. In other words, parameterisations that imply dryness changes can never modify burned area by more than 1%, regardless of the severity of the weather conditions, are assigned zero probability.

$$P\left(\{\beta_p\}|\{BF_i\},\{X_{i,v}\}\right) \propto P(\{\beta_p\}) \times \prod_{i}^{cell} \begin{cases} P(BF_i \mid \{\beta_p\},\{X_v\}) & if\ \dfrac{\Sigma_i f(\{X_v\}_{dryness}, \{\beta_p\}_{dryness}\}}{ncells} < 0.99 \\ 0 & otherwise \end{cases}$$

### S1.2.4. Future Projections - Typical Fire Behaviour

Whilst the current report focuses on 2025/2026 extreme fires, the Haas et al. (2026) GLMs were derived to represent the large-scale changes in median conditions of BA, fire size and fire intensity. As such, the projections here represent simulated increases or decreases in the median fire activity. They do not simulate how the distribution will change, nor do they simulate extreme events. This analysis aimed to determine whether a clear qualitative trend could be identified for any of the focal regions of properties beyond burned area, notably fire size and fire intensity. Given that the model outputs were computed at a 50km resolution, the ability of the models to reproduce fine-scale detail is limited and the outputs remain fairly coarse relative to the region size. This introduces systematic uncertainty, as the subpixel landscape and vegetation features will not be represented accurately. Furthermore, the 2010-2020 baseline was run using simulated vegetation cover from BIOME4 (Kaplan et al., 2003) and the P-Model (Stocker et al., 2020). This means that vegetation was driven by climate drivers alone, and does not capture observed land fractions, such as plantations or human land use. Nevertheless, it provides an evaluation of the current state-of-the-art fire size and intensity global models, and highlights the need for improvement and higher resolution regional modeling.

**Table S6:** Evaluation of the Haas et al. (2026) GLMs

| Focal region | Variable | Observations | Baseline | Bias | RMSE | Correlation | NME |
|---|---|---|---|---|---|---|---|
| Burned Area (BA) (reported as percent) | | | | | | | |
| Northwest Iberia | BA | 0.075% | 0.23% | 0.001 | 0.003 | 0.06 | 3.04 |
| Canada | BA | 0.11% | 0.37% | 0.002 | 0.003 | -0.11 | 1.32 |
| Chile | BA | 0.037% | 0.24% | 0.002 | 0.003 | 0.19 | 4.07 |
| Fire Size (FS) $km^2$ | | | | | | | |
| Northwest Iberia1 | FS | 1.78 $km^2$ | 0.33 $km^2$ | -1.44 | 2.164 | 0.64 | 0.85 |
| Canada2 | FS | 7.85 $km^2$ | 4.29 $km^2$ | -3.56 | 11.710 | 0.04 | 0.99 |
| Chile3 | FS | 3.02 $km^2$ | 0.91 $km^2$ | -2.11 | 4.843 | -0.04 | 1.04 |
| Fire Intensity (FI) $W.km^2$ | | | | | | | |
| Northwest Iberia | FI | 33.64 $W.km^2$ | 15.83 $W.km^2$ | -17.81 | 28.401 | -0.15 | 1.68 |
| Canada | FI | 49.01 $W.km^2$ | 40.61 $W.km^2$ | -8.41 | 74.081 | -0.04 | 1.01 |
| Chile | FI | 30.45 $W.km^2$ | 23.84 $W.km^2$ | -6.61 | 29.243 | -0.07 | 1.27 |

The Haas et al. GLM demonstrates the strongest and most consistent performance in Chile and Canada, particularly for burned area and best performance in Iberia for fire size (**Table S6**). For burned area, Chile shows acceptable performance in mean prediction and correlation, with moderate spatial agreement between modelled and observed patterns (spatial correlations ~0.2) and no systematic bias. However, the normalised mean square error is very large, meaning that the amplitude of the predictions varies greatly. This may be problematic for future projections. Canada also performs reasonably well, likely reflecting the model's ability to capture large-scale climatic controls and relatively homogeneous fuel structures. There does appear to be a systematic underestimation in the north-western region. In contrast, Iberia highlights key limitations. These results suggest that burned area is sensitive to vegetation representation, particularly in heterogeneous landscapes. Improving fuel and vegetation detail, as well as training or running the model at higher spatial resolution, could substantially improve performance in regions like Iberia. Fire size broadly follows the same regional performance patterns as burned area, with strong skill in Iberia, Chile and Canada and weaker performance in more heterogeneous regions. However, fire size is more strongly governed by fuel-related factors, particularly fuel continuity and fragmentation (e.g. landscape structure, roads, agricultural boundaries) which tend to be more stable in both present-day and projected future conditions. This relative stability in fuel fragmentation patterns may contribute to more consistent predictions in fire size compared to fire intensity, although projection confidence remains moderate and region-dependent. Fire intensity is the most challenging variable for the model to capture. The model is highly sensitive to long-term drought effects, particularly through its influence on vegetation and fuel accumulation. In the current setup, reduced seasonal fuel accumulation under prolonged drought leads to declining projected fire intensity, which may not fully reflect real-world dynamics where drought can also increase flammability. Fire intensity projections carry greater uncertainty than burned area and fire size. This uncertainty highlights that fire intensity responses to drought are likely region-dependent and poorly captured in the current modelling framework. This reflects both limitations in representing vegetation processes and their interaction with long-term dryness, and the challenge of resolving fine-scale variability at larger model scales. In Chile, there are also somewhat promising signals in fire intensity, although performance for intensity is consistently weaker than for the other two metrics. Across all regions, model skill varies depending on the fire characteristic being assessed, reflecting differences in the dominant controls on burned area, fire size, and intensity.

# S2. Global Extreme Wildfire Events of 2025-26

## S2.1. Supplementary Analysis: Cross-Product Intercomparison of Regional Burned Area Totals

To characterise the dependence of our findings on BA product choices, we add a supplementary comparison between the regional BA totals detected by the MCD64A1 BA product and two other BA products (**Figure S1**). The first comparison product was the ESA Climate Change Initiative Harmonised Medium Resolution Burned Area Grid product version 6.0 (MRBA60H). MRBA60 is a new harmonised global burned area dataset that extends the ESA FireCCI record from 2003 to the present at monthly 0.25° resolution. From 2019 onwards, MRBA60 uses the FireCCIS311 (Lizundia-Loiola et al., 2022) grid product directly, which is derived from Sentinel-3 SYN surface reflectance, combining OLCI and SLSTR reflectance, and guided by VIIRS active fire detections through a contextual algorithm at 300 m resolution. For 2003-2018, MRBA60 is based on the long-term MODIS-derived FireCCI51 record (Lizundia-Loiola et al., 2020), but uses biome and season specific Random Forest models to predict burned area values harmonised with the higher resolution Sentinel-3 based FireCCIS311 product. These models were trained over the 2019-2024 overlap between FireCCI51 and FireCCIS311, with additional predictors including active fires, fire radiative power, climate and vegetation indices (Torres-Vazquez et al., 2026). The second comparison product is NASA's VIIRS BA product (VNP64A1 v002; Giglio et al., 2025), generated using an adaptation of the MODIS MCD64A1 Collection 6.1 algorithm, applied to 750 m VIIRS imagery and active fire detections. The hybrid algorithm uses dynamic thresholds on composite imagery derived from a burn-sensitive vegetation index and temporal texture measures, enabling it to distinguish fire-induced changes from other land surface changes. It identifies the burn date at 500 m resolution for each grid cell, with prior probabilities of burned/unburned areas informed by cumulative VIIRS active fire observations.

The VIIRS VNP64A1 product has been available since 2013 only, and hence our cross-product comparisons focus on the fire seasons March 2013-February 2026. We followed identical approaches as described in **Section 2.1.2** to calculate regional BA totals and to quantify anomalies of the past fire season.

With very few exceptions, we find a high level of consistency between the MCD64A1, FireCCIS311, and VIIRS VNP64A1 BA products with regards to both the relative magnitude of regional BA anomalies, the geographical distribution of those anomalies, and the rankings of BA in the 2025-26 fire season versus previous fire seasons since 2019 (**Figure S1**). This analysis adds confidence that regional anomalies identified in the MCD64A1 BA product are consistent across products from different space agencies using different algorithms applied to different combinations of Earth-observing sensors. The MCD64A1 BA product will soon discontinue due to the decommissioning of MODIS sensors aboard NASA's Terra and Aqua satellites, and the consistency across products is an encouraging finding for the continuity of our annual reporting.

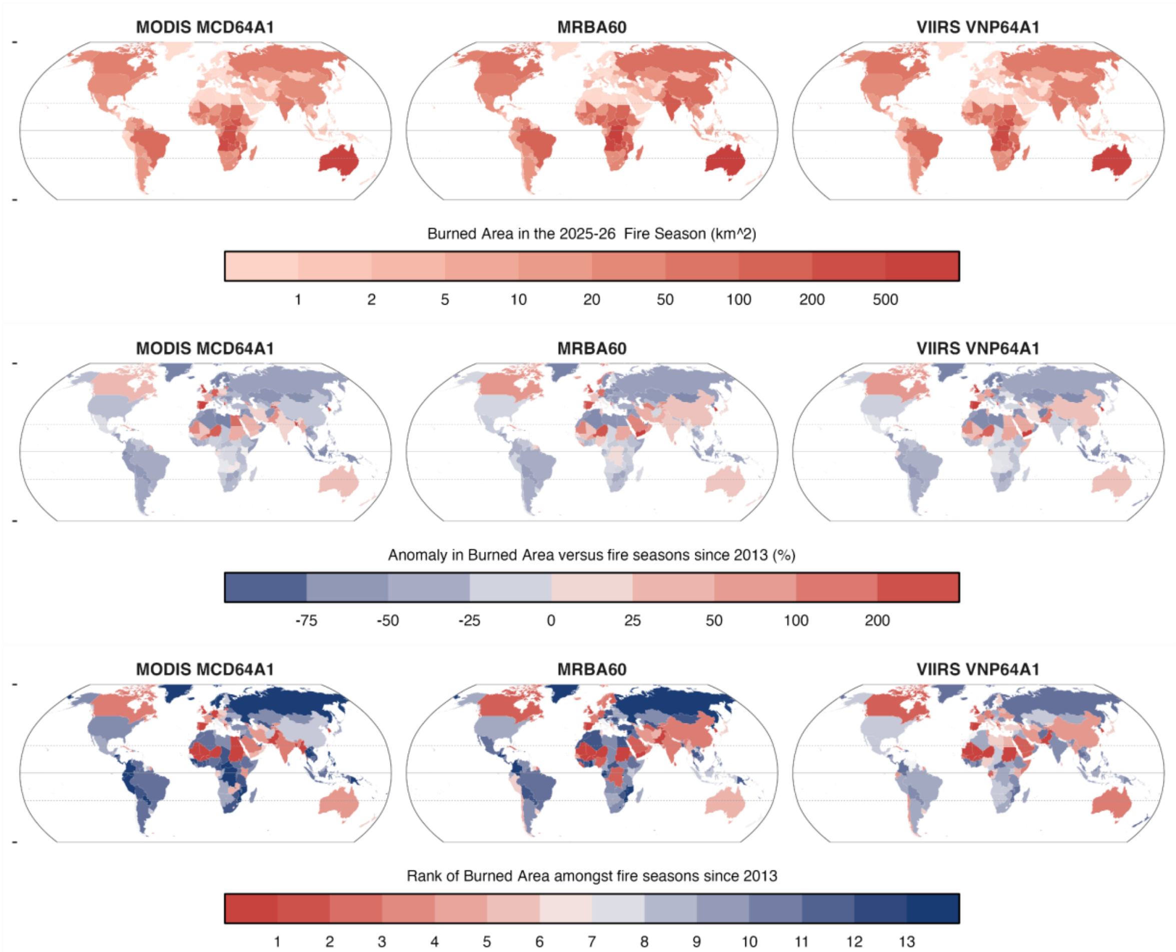


**Figure S1:** Comparison of the burned area (BA) estimates from **(left column)** the ESA Climate Change Initiative FireCCI Harmonised Medium Resolution Burned Area Grid product version 6.0 (MRBA60H; Torres-Vazquez et al., 2026), **(middle column)** the VIIRS BA product produced by NASA (VNP64A1 v002) (Giglio, 2024; Zubkova et al., 2024) and **(right column)** the MODIS BA product produced by NASA (MCD64A1 collection 6.1; Giglio et al., 2018).

## S2.2. Supplementary Analysis: Contemporaneous Extremes in Fire Weather

As in last year's report, we produce routine summaries of the extreme (95$^{th}$ percentile) fire weather days during the March 2025-February 2026 global fire season based on the FWI, a common metric of fire danger developed by the Canadian Forest Service as part of the Canadian Forest Fire Danger Rating System (CFFDRS; van Wagner, 1987). The FWI comprises various components that consider the influence of weather on fire danger, with 2m temperature, 10m wind speed, precipitation, and 2m relative humidity as prerequisite variables. Higher FWI values are generally seen during droughts, heatwaves and strong winds as these conditions are conducive to wildfires in environments with sufficient fuel load (Jolly et al., 2015; Di Giuseppe, 2016; Jones et al., 2022). We base our analysis of extreme (95th percentile) fire weather on the FWI dataset derived from the Copernicus Climate Change Service ERA5 reanalysis (Hersbach et al., 2020; Vitolo et al., 2020) and maintained by the Copernicus Emergency Management Service (CEMS, version 4.1, 2019). The 95th percentile value for extreme fire weather has been used in many prior publications (e.g., Abatzoglou et al., 2019; Jones et al., 2022). The same statistics are reported for the 2025-26 fire season as in the case of fire observational datasets, including (i) ranks, (ii) proportional anomalies, and (iii) standardised anomalies amongst all fire seasons since 2002 (**Figure S2**).

We no longer comment at length on the results of this analysis, but recognise that the data may be of value to certain end users. The data produced using these methods are available from Turco et al. (2026).

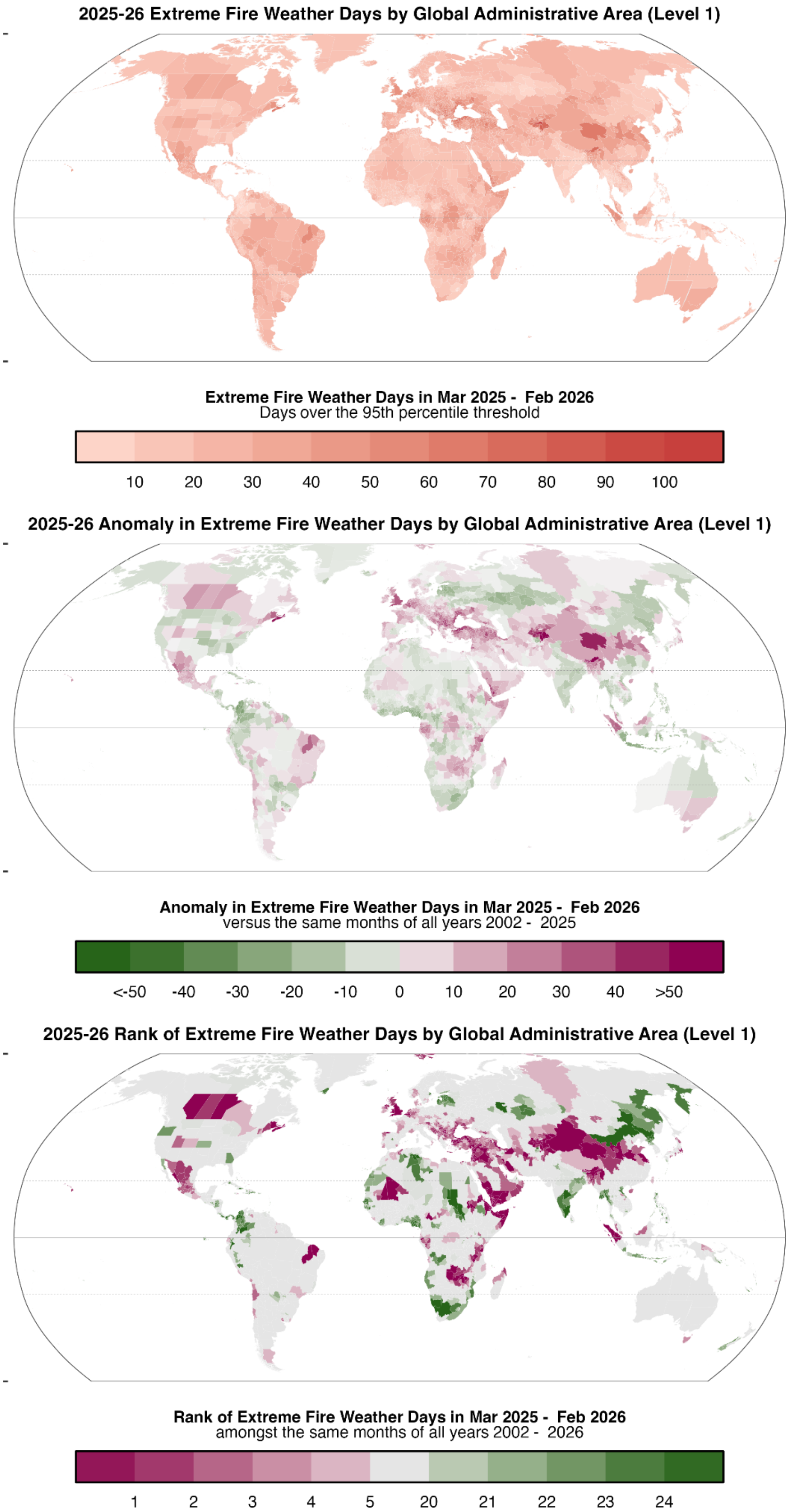


**Figure S2:** Extreme fire weather in the past fire season, including **(top panel)** the number of days with extreme (95th percentile) fire weather during the 2025-26 fire season, **(middle panel)** the anomaly versus the mean of all prior fire seasons 2002-2025, and **(bottom panel)** rank amongst all fire seasons since 2002.

## S2.3. Supplementary Analysis: 21st Century Trends in Burned Area

To place recent extremes in the context of fire trends of the past two decades, we update our regional analyses of trends in annual BA from Jones et al. (2022). In addition to reporting trends in *total* BA, we also present trends in *forest* BA as these regularly diverge from total BA trends (**Figure S3**), following Jones et al. (2024a).

We no longer comment at length on the results of this analysis, but recognise that the data may be of value to certain end users. The data produced using these methods are available from Jones et al. (2026).

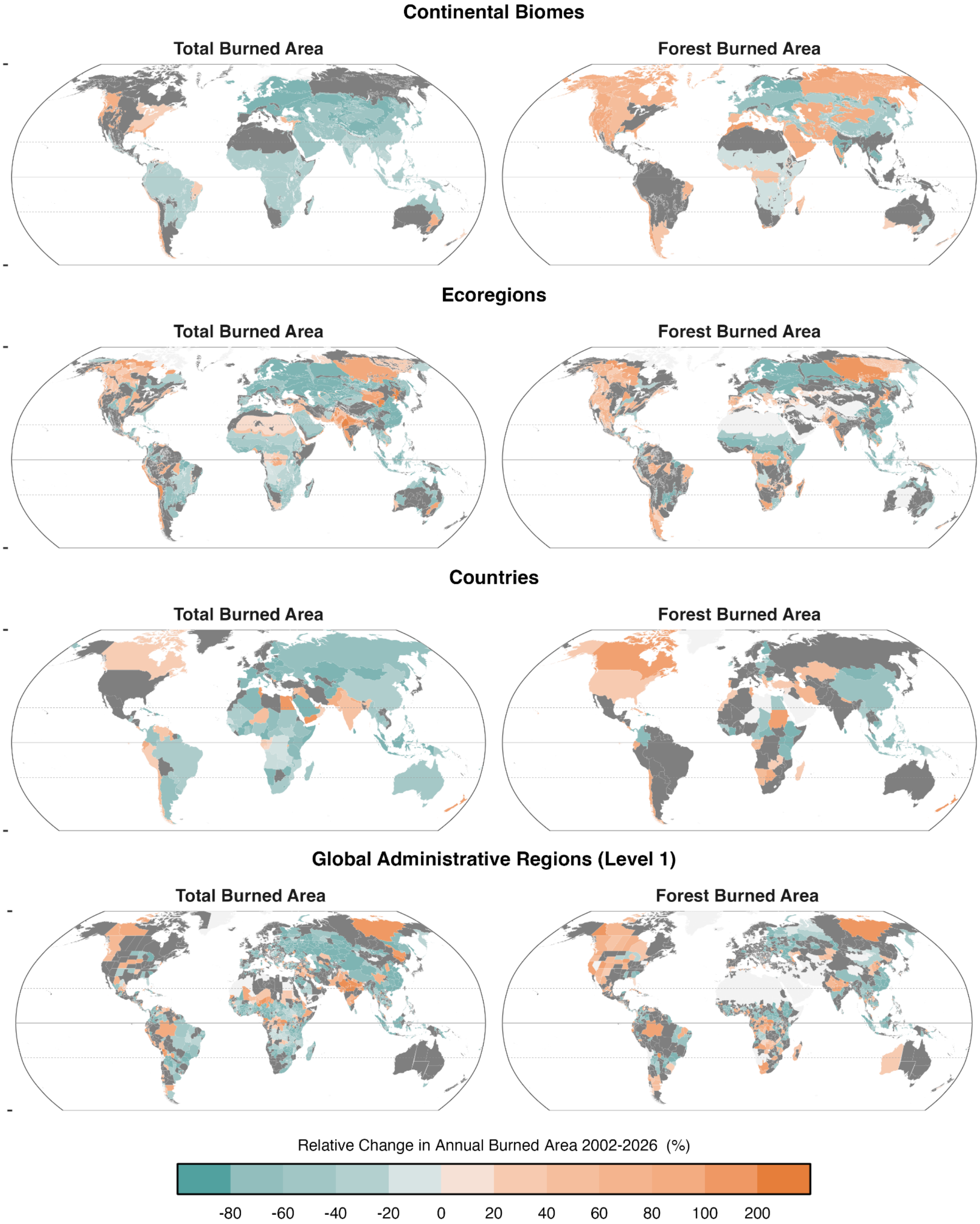

**Figure S3:** Relative changes (%) in **(left panels)** total annual BA and **(right panels)** forest BA across March-February fire seasons during 2002-2025 for three regional layers: **(top panels)** continental biomes; **(middle panels)** countries, and **(bottom panels)** level 1 administrative regions (e.g., states or provinces). Forest BA considers only areas with tree cover over 30% at the native (500 m) resolution of the BA observations. Relative changes are calculated as the trend in BA across fire seasons March 2002-February 2003 through March 2025-February 2026 multiplied by the number of years in the time series and divided by the mean annual BA during the period. Trends in BA are derived using the Theil-Sen slope estimator. Only significant trends ($p < 0.05$) in BA are shown (dark grey fill signifies no significant trend).

## S2.4. Supplementary Analysis: Drought Conditions and Carbon Project Exposure

Drier-than-average conditions were observed across many project regions in 2025, with negative SPEI anomalies recorded in most regions. Over all projects, the SPEI anomaly was 0.52 lower than the 1980-2024 average. Considering that the 2025 fire impact on forest carbon projects was below average even as drought conditions worsened, drought alone could not explain fire exposure. Other factors, such as fuel availability, ignition sources, land-use change, and management practices (e.g. fire-suppression) are crucial in understanding project exposure to fire.

## S2.5. Extended Supplementary Figures

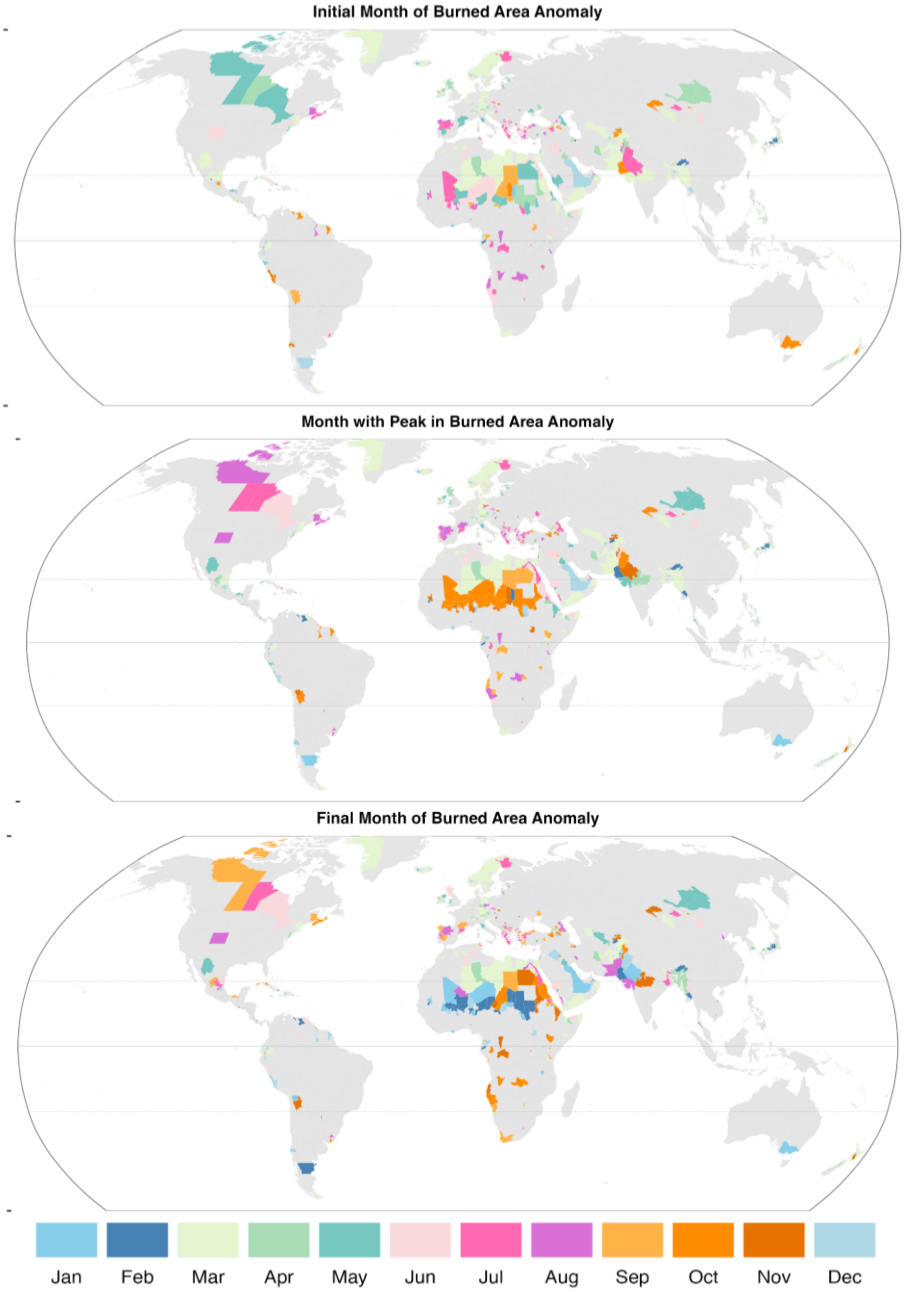


**Figure S4: (Top panel)** first month, **(middle panel)** peak month, and **(lower panel)** final month of positive BA anomalies at Global Administrative Level 1 during March 2025-February 2026. Peak anomalies are identified relative to the monthly climatology in 2001-2025. The first and final months of the BA anomaly incorporate the period when BA was continuously above the climatological mean. Graduated colours are separated seasonally.

# S3. Focal Region 1: Midwestern Canadian Shield Forests

## S3.1 Influence of Climate Change

### S3.1.1 Changes in Fire Weather

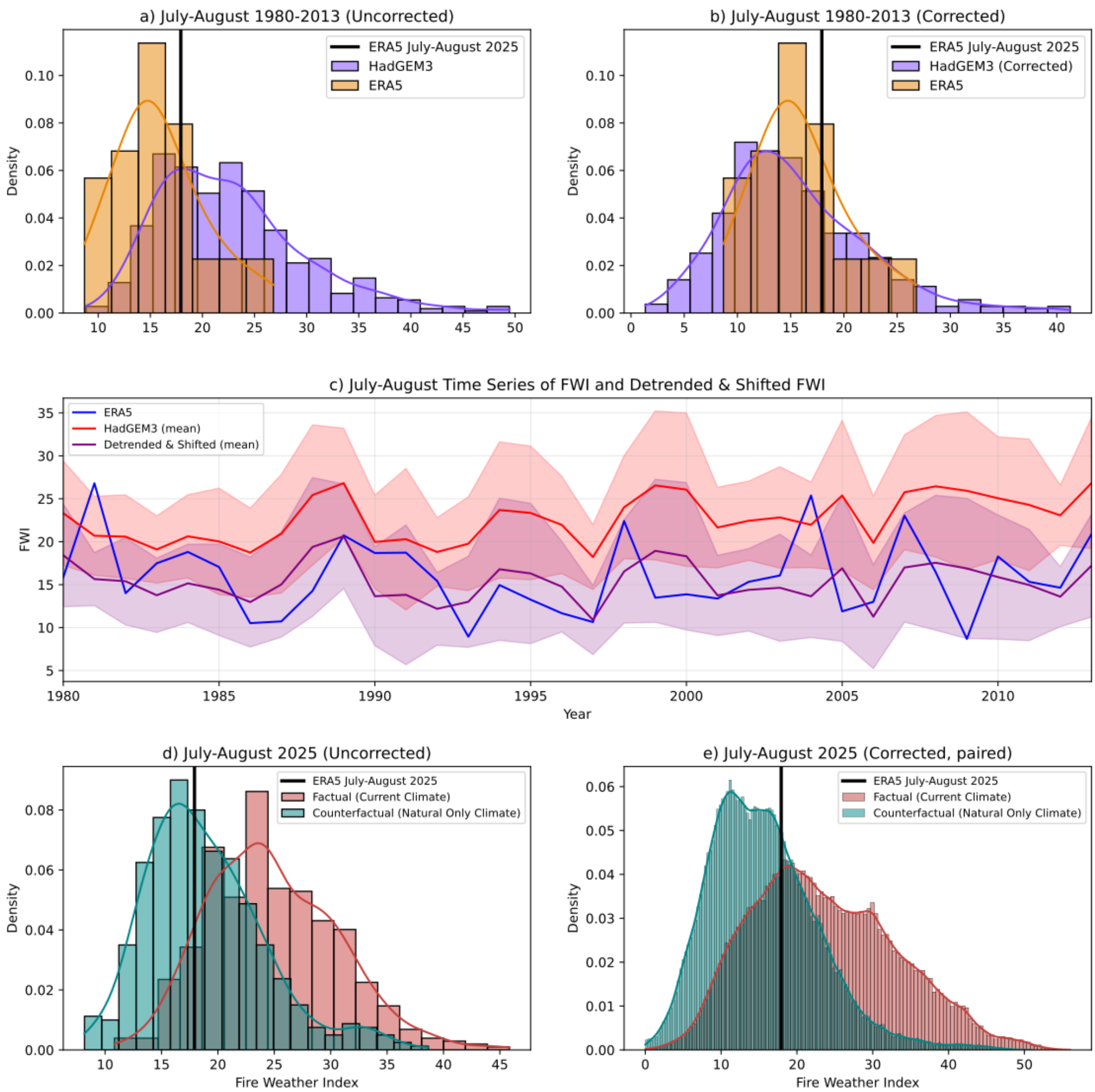


**Figure S5: HadGEM3-A Bias Correction. (a)**: Histogram of uncorrected reanalysis (ERA5) and historical ensemble (HadGEM3-A) results for FWI 95th percentile values for months July-August during the period 1980-2013. Black line denotes the reanalysis value for the FWI 95th percentile value during the event period: July-August 2025 (**FWI = 17.9**). **(b)**: Histogram of corrected model and reanalysis results for FWI 95th percentile values for period July-August 1980-2013. **(c)**: Time-series of uncorrected (red), corrected (purple) model and reanalysis (blue) July-August FWI 95th percentile values for period 1980-2013. Solid Red and Purple lines denote 15 member mean, shading denotes 1std. **(d)**: Uncorrected 525 member attribution ensemble histogram for FWI 95th percentile for 2020-2024, teal representing natural only climate (Counterfactual), red denoting anthropogenically altered climate (Factual). **(e)**: Bias corrected 7875 (525 * 15) member attribution ensemble histogram for 2020-2024, colours assignment unchanged.

**Figure S5** details the bias correction applied to the Factual and Counterfactual ensembles as summarised in **S1.2.1**. The uncorrected historical ensemble tends to overestimate the FWI with respect to the reanalysis FWI for the same period (panels a and c). The adjustment corrects for the trend and absolute value (panels b and c). We then apply this bias correction to the present day ensemble to calculate the PR (panel e). With respect to the reanalysis baseline period of 1980-2013, the FWI95 seen during the event in July-August 2025 was slightly above average. During the baseline period the mean FWI95 from ERA5 was 15.9 versus the event value of 17.9. This represents a 13% percent increase over climatology.

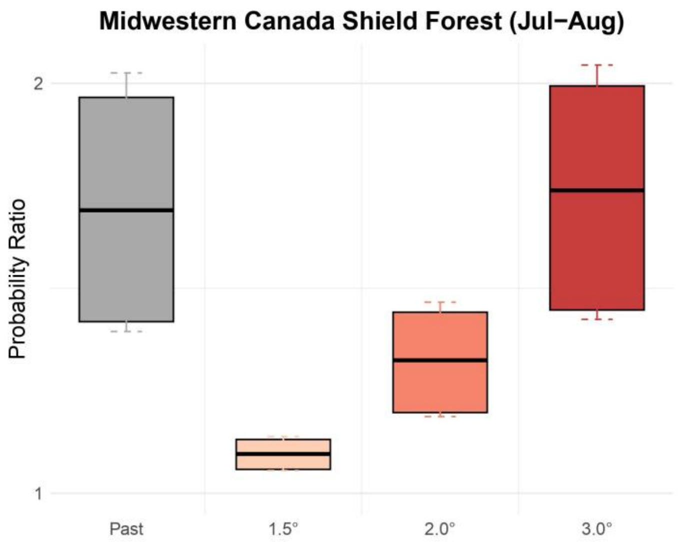


**Figure S6:** Probability Ratio (PR) estimates based on the comparison between (a) the past climate of 1850-1859 and the recent climate of 2017-2026, the recent climate of 2017–2026 and the period that global mean surface temperature (GMST) reached 1.5 °C, 2 °C and 3 °C for Midwestern Canadian Shieldforests using FWI7X. Results are synthesised based on CanESM5, ACCESS-ESM1-5, and MPI-ESM1-2-LR from CMIP6 models with large (>10) climate ensembles. A 1000-sample non-parametric bootstrapping method is used to give uncertainty estimates for the FWI7X PRs. Bars show 5-95th confidence intervals (CIs), whiskers show 2.5th and 97.5th percentiles, and central values are shown by bold horizontal lines.

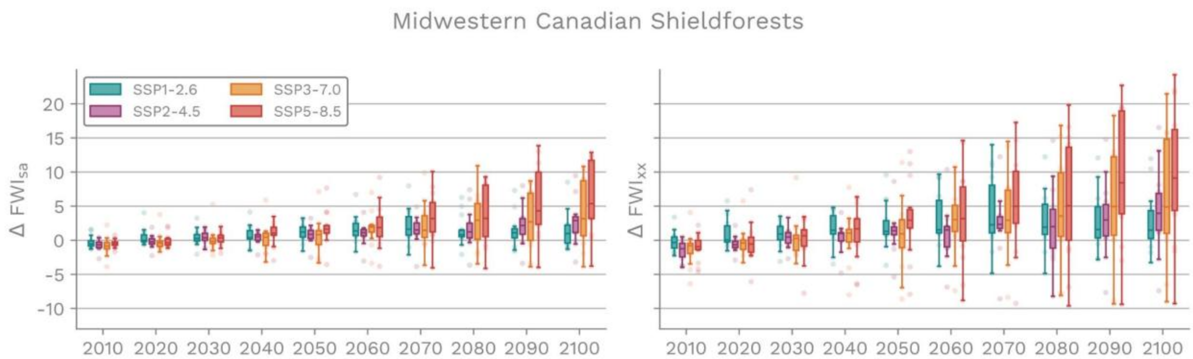


**Figure S7:** Projected changes in seasonal mean ($FWI_{sa}$; left) and annual maxima ($FWI_{xx}$; right) Fire Weather Index (FWI) for the Midwestern Canadian Shield Forests under CMIP6 SSP scenarios, with respect to the reference period 2010-2020. Boxplots show the distribution across CMIP6 models for each decade, with coloured points indicating individual CMIP6 model results, while boxes represent the interquartile range (25th–75th percentiles).

### S3.1.2 Changes in Burned Area

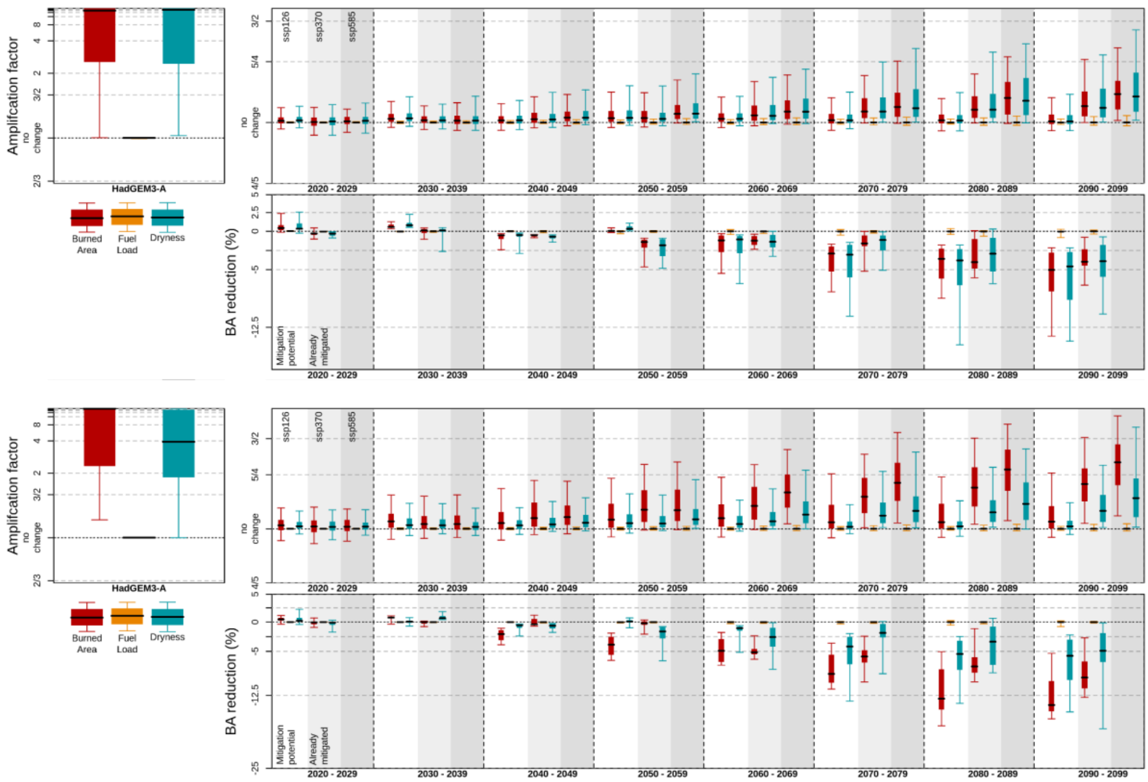


**Figure S8:** Top two panels per Figure 10 with future projections shown for each decade. Bottom two panels show attribution and projections for sub-regional extremes, i.e for grid cells with top 5% burned area.

**Table S7: Focal event burned area attribution and projection results** for present day and Shared Socioeconomic Pathway (SSP) scenarios. Colours denote likelihood based on IPCC definitions. Best estimate shown in bold, with 5-95th percentiles in brackets. Mitigation shows the % differences between SSP5-8.5 and SSP3-7.0 AF (in SSP3-7.0 columns) and SSP3-7.0 and SSP1-2.6 (in SSP1-2.6 columns), expressed as 100x (1-lower/high emissions BA).

| | | Present | SSP1-2.6 | | | SSP3-7.0 | | | SSP5-8.5 | | |
|---|---|---|---|---|---|---|---|---|---|---|---|
| | | | ***2030s*** | ***2040s*** | ***2090s*** | ***2030s*** | ***2040s*** | ***2090s*** | ***2030s*** | ***2040s*** | ***2090s*** |
| **BA** | *Probability Ratio* | **61.41** (0.96, >100) | **1** (0.98, 1.04) | **1** (0.98, 1.05) | **1** (0.98, 1.06) | **1** (0.98, 1.04) | **1** (0.98, 1.07) | **1.02** (0.99, 1.18) | **1** (0.98, 1.04) | **1.01** (0.99, 1.06) | **1.05** (0.99, 1.28) |
| | *Likelihood* | 95 | 68 | 63 | 64 | 61 | 66 | 86 | 59 | 72 | 91 |
| | *Amplification factor* | **45.84** (1, >100) | **1.01** (0.99, 1.09) | **1.01** (0.97, 1.09) | **1.01** (0.97, 1.09) | **1.01** (0.98, 1.06) | **1.01** (0.98, 1.1) | **1.06** (1, 1.25) | **1.01** (0.97, 1.08) | **1.02** (0.99, 1.1) | **1.11** (1.01, 1.37) |
| | *Likelihood* | 97 | 82 | 67 | 60 | 69 | 73 | 95 | 67 | 84 | 97 |
| | *Mitigation* | | **0.74** (3.21, 0.54) | **-0.49** (-0.26, -2.11) | **-5.16** (-2.54, -12.39) | **-0.05** (0.38, -0.05) | **-0.56** (0, -0.92) | **-4.66** (-0.68, -8.7) | | | |
| | *Likelihood* | | 0 | 99 | 100 | 54 | 91 | 100 | | | |
| **Fuel** | *Amplification factor* | **1** (1, 1) | **1** (1, 1) | **1** (1, 1.01) | **1** (0.99, 1.01) | **1** (1, 1.01) | **1** (1, 1.01) | **1** (0.99, 1.02) | **1** (1, 1.01) | **1** (1, 1.01) | **1** (0.99, 1.02) |
| | *Likelihood* | 45 | 50 | 54 | 57 | 56 | 57 | 57 | 57 | 57 | 57 |
| | *Mitigation* | | **-0.02** (0, -0.08) | **-0.01** (0, -0.01) | **-0.01** (-0.91, 0.41) | **-0.01** (-0.13, 0.02) | **0** (-0.21, 0.08) | **0** (-0.38, 0.24) | | | |
| | *Likelihood* | | 99 | 94 | 57 | 85 | 58 | 53 | | | |
| **Dryness** | *Amplification factor* | **91.76** (1.02, >100) | **1.01** (0.99, 1.09) | **1.01** (0.98, 1.09) | **1** (0.97, 1.11) | **1.01** (0.98, 1.07) | **1.01** (0.99, 1.12) | **1.05** (1, 1.3) | **1.01** (0.98, 1.1) | **1.02** (0.99, 1.12) | **1.1** (1.01, 1.45) |
| | *Likelihood* | 98 | 85 | 69 | 56 | 71 | 77 | 97 | 66 | 87 | 98 |
| | *Mitigation* | | **0.96** (2.07, 0.65) | **-0.25** (-0.07, -0.25) | **-4.55** (-14.75, -2.33) | **-0.04** (-2.76, 0.38) | **-0.69** (-1.49, -0.4) | **-4.24** (-10.3, -0.58) | | | |
| | *Likelihood* | | 0 | 100 | 100 | 52 | 97 | 100 | | | |

| Virtually Certain | Very Likely | Likely | About as likely as not | Unlikely | Very Unlikely | Extremely Unlikely |
|---|---|---|---|---|---|---|
| >99% | >90% | >66% | 33-66% | <33% | <10% | <1% |

**Table S8: Sub-regional burned area extremes attribution and projection results**. Sub-regional extremes defined as the grid cells with top 5% BA. Otherwise as per Table S7

| | | Present | SSP1-2.6 | | | SSP3-7.0 | | | SSP5-8.5 | | |
|---|---|---|---|---|---|---|---|---|---|---|---|
| | | | *2030s* | *2040s* | *2090s* | *2030s* | *2040s* | *2090s* | *2030s* | *2040s* | *2090s* |
| **BA** | *PR* | **>100** (1.13, >100) | **1.01** (0.96, 1.09) | **1.01** (0.96, 1.08) | **1.02** (0.98, 1.16) | **1.01** (0.97, 1.09) | **1.03** (0.98, 1.17) | **1.1** (1, 1.63) | **1.01** (0.97, 1.11) | **1.03** (0.98, 1.15) | **1.28** (1.02, 1.7) |
| | *Likelihood* | 96 | 73 | 70 | 77 | 72 | 83 | 99 | 72 | 84 | 100 |
| | *AF* | **>100** (1.16, >100) | **1.03** (0.96, 1.13) | **1.03** (0.96, 1.18) | **1.03** (0.97, 1.26) | **1.02** (0.96, 1.12) | **1.06** (0.97, 1.26) | **1.23** (1.04, 1.52) | **1.02** (0.96, 1.13) | **1.06** (0.98, 1.25) | **1.27** (1.05, 1.58) |
| | *Likelihood* | 97 | 79 | 77 | 80 | 71 | 86 | 99 | 71 | 89 | 100 |
| | *Mitigation* | | **0.9** (1.52, -0.02) | **-2.46** (-1.22, -6.59) | **-15.73** (-6.67, -17.12) | **-0.07** (0.15, -0.07) | **-0.25** (0, -1.67) | **-3.03** (-1.94, -3.78) | | | |
| | *Likelihood* | | 5 | 100 | 100 | 56 | 55 | 100 | | | |
| **Fuel** | *AF* | **1** (1, 1) | **1** (1, 1) | **1** (1, 1.01) | **1** (0.99, 1.01) | **1** (1, 1) | **1** (1, 1.01) | **1** (0.99, 1.02) | **1** (1, 1) | **1** (1, 1.01) | **1** (0.99, 1.02) |
| | *Likelihood* | 44 | 58 | 56 | 54 | 59 | 57 | 54 | 58 | 58 | 55 |
| | *Mitigation* | | **0** (0.01, -0.04) | **0** (0.02, 0) | **0** (-0.79, 0.23) | **0** (-0.08, 0.03) | **0** (-0.14, 0.04) | **-0.01** (-0.35, 0.14) | | | |
| | *Likelihood* | | 80 | 84 | 51 | 55 | 65 | 61 | | | |
| **Dryness** | *AF* | **4.67** (1, >100) | **1.02** (0.99, 1.11) | **1.01** (0.98, 1.1) | **1.01** (0.98, 1.1) | **1.01** (0.98, 1.09) | **1.01** (0.99, 1.1) | **1.06** (1, 1.32) | **1.01** (0.98, 1.08) | **1.02** (0.99, 1.13) | **1.12** (1, 1.48) |
| | *Likelihood* | 98 | 81 | 73 | 65 | 75 | 82 | 98 | 63 | 87 | 97 |
| | *Mitigation* | | **0.8** (2.29, 0.18) | **-0.13** (0.27, -0.13) | **-4.93** (-2.14, -16.73) | **0.42** (0.35, 0.75) | **-0.75** (-0.16, -2.35) | **-5.37** (-0.01, -10.07) | | | |
| | *Likelihood* | | 0 | 69 | 100 | 1 | 99 | 95 | | | |

### S3.1.3 Changes in Typical Fire Behaviour

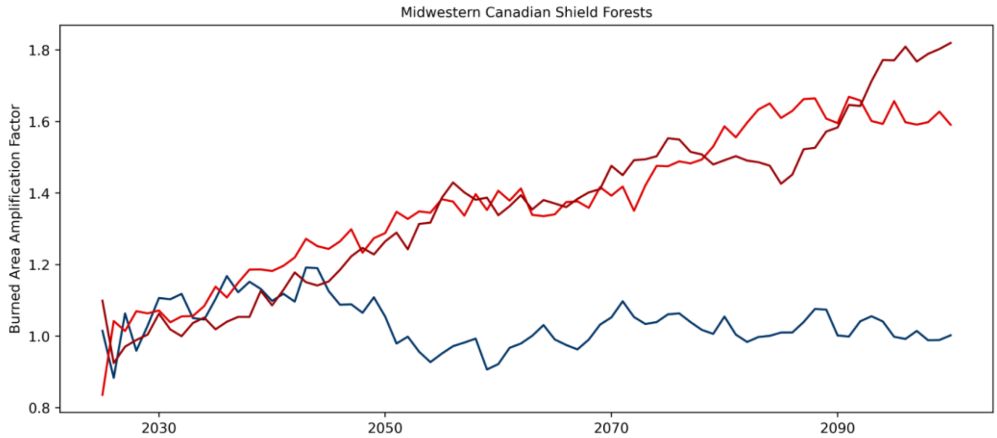


**Figure S9**: Future projections of burned area (BA) amplification factors (AF) from BuRNN for the 2025-2100 period, considering several Shared Socioeconomic Pathway (SSP) scenarios: SSP1-2.6 (blue), SSP3-7.0 (orange) and SSP5-8.5 (red).

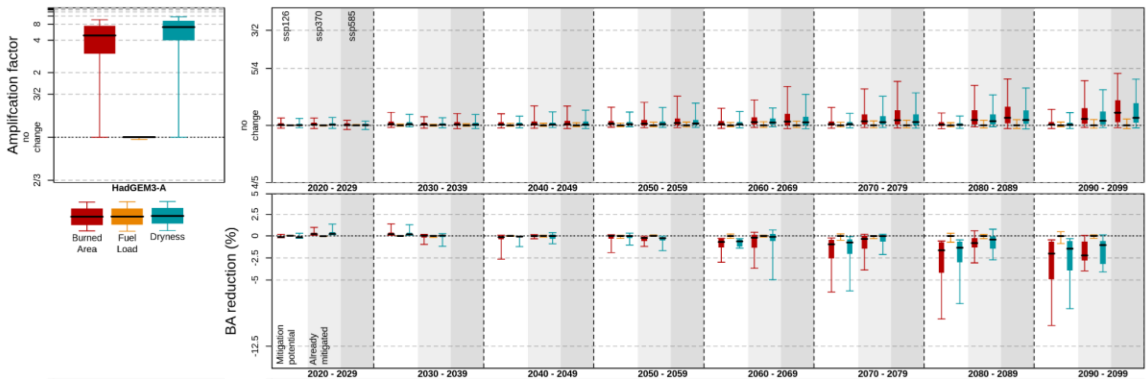


**Figure S10:** Same as **Figure 10** for decade average burned area.

**Table S9: Annual average burned area attribution and projection results**. Otherwise, as per **Table S7**

| | | Present | SSP1-2.6 | | | SSP3-7.0 | | | SSP5-8.5 | | |
|---|---|---|---|---|---|---|---|---|---|---|---|
| | | | *2030s* | *2040s* | *2090s* | *2030s* | *2040s* | *2090s* | *2030s* | *2040s* | *2090s* |
| **BA** | ***BURRN*** | | 1.13 | 1.11 | 0.99 | 1.19 | 1.27 | 1.63 | 1.13 | 1.23 | 1.8 |
| | *PR* | **5.94** (0.87, 32.73) | **1** (1, 1.01) | **1** (1, 1.01) | **1** (1, 1.03) | **1** (1, 1.01) | **1.01** (1, 1.02) | **1.0** (1.02, 1.14) | **1** (1, 1.01) | **1** (1, 1.02) | **1.04** (1.04, 1.18) |
| | *Likelihood* | 94 | 100 | 80 | 100 | 100 | 100 | 100 | 80 | 100 | 100 |
| | *AF* | **4.7** (1, 10.91) | **1.01** (0.99, 1.05) | **1** (0.99, 1.04) | **1** (0.99, 1.08) | **1** (0.99, 1.03) | **1.01** (0.99, 1.08) | **1.03** (0.99, 1.2) | **1** (0.99, 1.04) | **1** (0.99, 1.08) | **1.04** (0.99, 1.27) |
| | *Likelihood* | 97 | 79 | 67 | 66 | 74 | 72 | 85 | 69 | 67 | 89 |
| | *Mitigation* | | **0.19** (1.2, 0.11) | **-0.2** (-0.08, -3.22) | **-2.19** (-0.42, -9.51) | **0.06** (0.23, 0.06) | **0.04** (0, -0.12) | **-1.69** (0.1, -5.45) | | | |
| | *Likelihood* | | 0 | 100 | 100 | 31 | 38 | 93 | | | |
| **Fuel** | *AF* | **1** (0.98, 1) | **1** (1, 1) | **1** (1, 1.01) | **1** (0.99, 1.01) | **1** (1, 1) | **1** (1, 1.01) | **1** (0.99, 1.02) | **1** (1, 1.01) | **1** (1, 1.01) | **1** (0.99, 1.02) |
| | *Likelihood* | 36 | 51 | 56 | 57 | 56 | 57 | 58 | 57 | 58 | 58 |
| | *Mitigation* | | **-0.02** (0, -0.05) | **0** (0.03, 0) | **-0.01** (-0.76, 0.3) | **0** (-0.17, 0.03) | **0** (-0.23, 0.06) | **0** (-0.42, 0.23) | | | |
| | *Likelihood* | | 96 | 66 | 61 | 61 | 64 | 61 | | | |
| **Dryness** | *AF* | **6.76** (1, 14.53) | **1** (1, 1.04) | **1** (0.99, 1.04) | **1** (0.99, 1.06) | **1** (0.99, 1.03) | **1** (0.99, 1.05) | **1.02** (0.99, 1.14) | **1** (0.99, 1.04) | **1** (0.99, 1.06) | **1.03** (0.99, 1.18) |
| | *Likelihood* | 96 | 76 | 66 | 60 | 71 | 72 | 83 | 63 | 66 | 87 |
| | *Mitigation* | | **0.22** (1.17, 0.08) | **-0.12** (-0.05, -0.12) | **-1.55** (-7.16, -0.3) | **0.05** (-0.98, 0.35) | **-0.01** (-1, 0.51) | **-1.13** (-3.6, 0.11) | | | |
| | *Likelihood* | | 0 | 100 | 100 | 19 | 52 | 94 | | | |

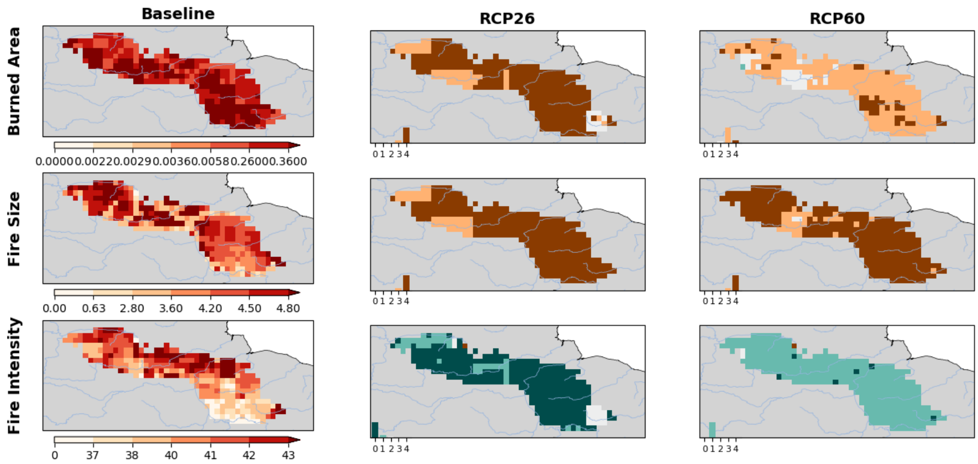


**Figure S11:** Projected changes in fire characteristics across ISMIP2b GMC future projections taken from Haas et al. (2026). The left column shows modelled baseline conditions for the 2010s, while the right columns show model agreement on the direction of change by 2100 under RCP2.6 (middle) and RCP6.0 (right). Colours indicate the number of models projecting an increase or decrease at each location (brown representing projected increases and blue representing projected decreases). The accompanying histograms (inset) summarise the spatial extent of agreement by showing the fraction of the region where a given number of models agree on the direction of change. Rows correspond (top to bottom) to burned area, fire size, and fire intensity.

# S4. Focal Region 2: Northwest Iberia

## S4.1. Influence of Climate Change

### S4.1.1. Changes in Fire Weather

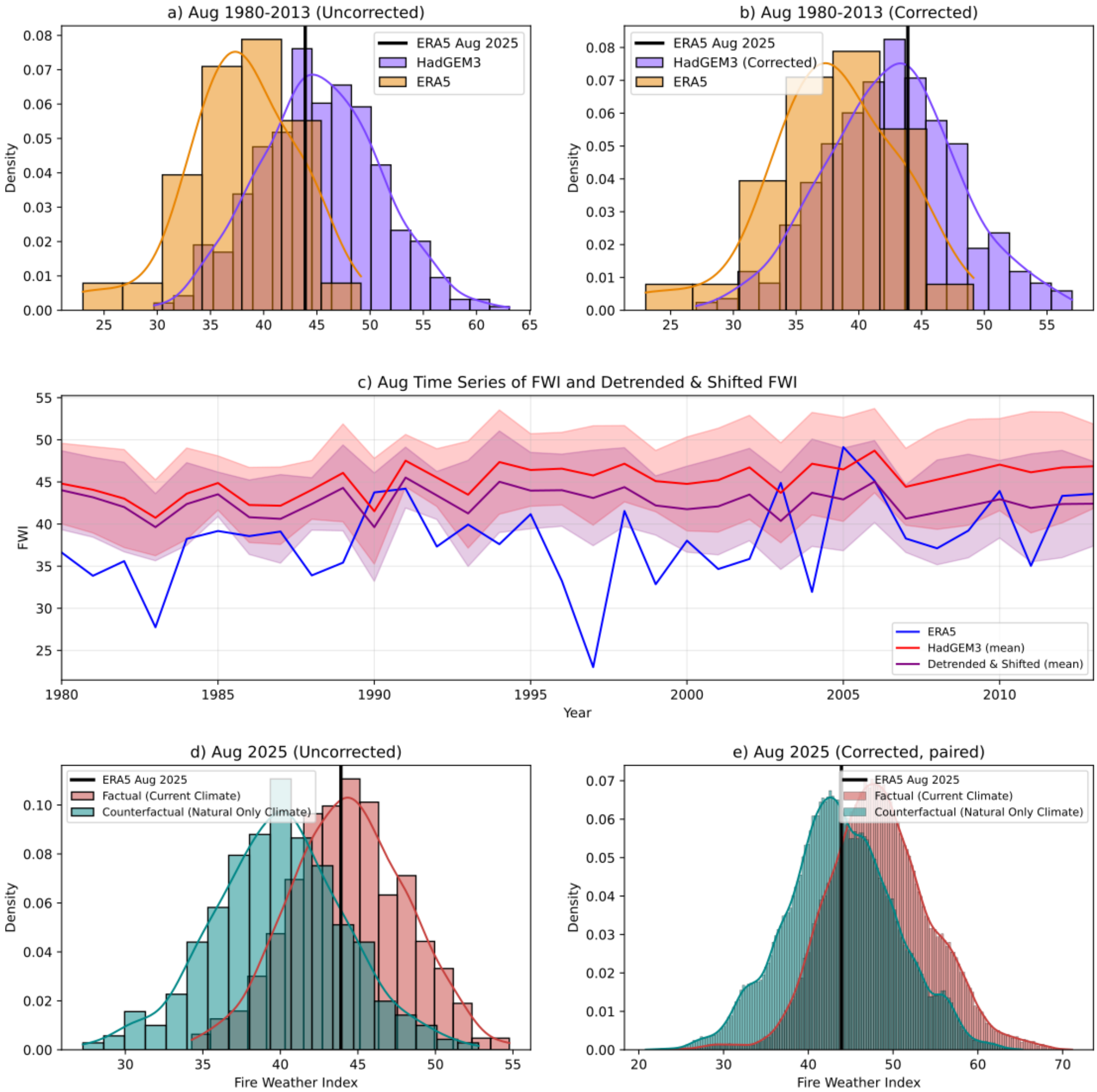


**Figure S12**: **HadGEM3-A Bias Correction. (a)**: Histogram of uncorrected reanalysis (ERA5) and model (HadGEM3) results for FWI 95th percentile values for August during the period 1980-2013. Black line denotes the ERA5 reanalysis value for the FWI 95th percentile value during the event period: **August 2025 (FWI = 43.9)**. **(b)**: Histogram of corrected model and reanalysis results for FWI 95th percentile values for August 1980-2013. **(c)**: Time-series of uncorrected (red), corrected (purple) model and reanalysis (blue) August FWI 95th percentile values for period 1980-2013. Solid Red and Purple lines denote 15 member mean, shading denotes 1std. **(d)** Uncorrected 525 member attribution ensemble histogram for FWI 95th percentile for 2020-2024, teal representing natural only climate, red denoting anthropogenically altered climate. **(e)** Bias corrected 7875 (525 * 15) member attribution ensemble histogram for 2020-2024, colours assignment unchanged.

**Figure S5.1** details the bias correction applied to the two attribution ensembles as summarised in **S2.5.1.** For this region too, the uncorrected historical ensemble tends to overestimate the FWI with respect to the reanalysis FWI for the same period (panels a and c). The model also underestimates variability in this region, however our bias adjustment only corrects for trend and absolute value (panel c). Therefore the effects of the bias correction were less pronounced here than in the other focal regions. While the bias correction improves the agreement of the distributions, there is a noticeable offset in the reanalysis and historical ensemble distributions (panel b). During the baseline period the mean FWI95 from ERA5 was 38.0. The FWI95 seen during the event in August 2025 was 43.9, representing a 15% increase over climatology.

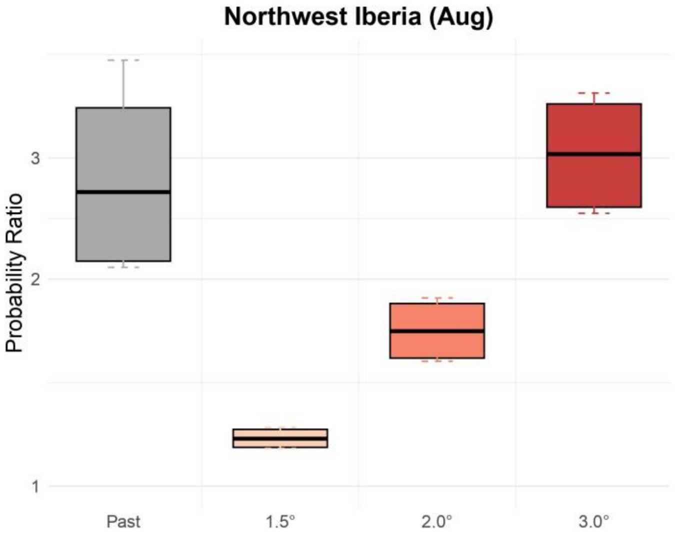


**Figure S13:** Probability Ratio (PR) estimates based on the comparison between (a) the past climate of 1850-1859 and the recent climate of 2017-2026, the recent climate of 2017–2026 and the period that global mean surface temperature (GMST) reached 1.5 °C, 2 °C and 3 °C for Northwest Iberia using FWI7X. Results are synthesised based on CanESM5, ACCESS-ESM1-5, and MPI-ESM1-2-LR from CMIP6 models with large (>10) climate ensembles. A 1000-sample non-parametric bootstrapping method is used to give uncertainty estimates for the FWI7X PRs. Bars show 5-95th confidence intervals (CIs), whiskers show 2.5th and 97.5th percentiles, and central values are shown by bold horizontal lines.

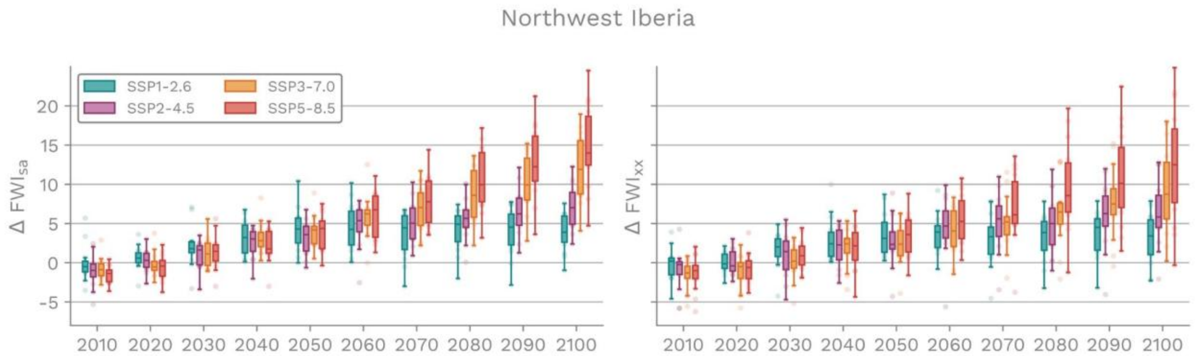


**Figure S14**: Projected changes in seasonal mean ($FWI_{sa}$; left) and annual maxima ($FWI_{xx}$; right) Fire Weather Index (FWI) for Northwest Iberia under CMIP6 SSP scenarios, with respect to the reference period 2010-2020. Boxplots show the distribution across CMIP6 models for each decade, with coloured points indicating individual CMIP6 model results, while boxes represent the interquartile range (25th–75th percentiles).

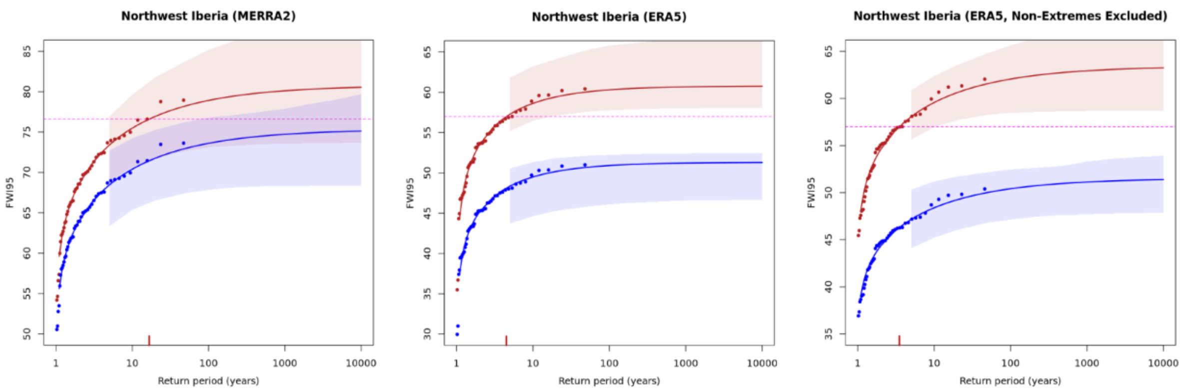


**Figure S15**: Statistical fits to FWI95. The influence of GMST is shown with the red vs blue probability curves, respectively showing all observed annual maxima as if they had occurred in the present climate (2025-26, red) vs pre-industrial warming levels (blue). The magnitude of the 2025-26 event is highlighted with a horizontal magenta line. Figures are given for the two reanalysis datasets (MERRA2, left, and ERA5, centre), and for ERA5 excluding two low values (right).

**Figure S15** shows that across datasets, the PR between preindustrial and present climates is infinite for the central estimate. The CI on the ERA5 return period appears narrow at the upper bound. This is due to the effect of two low values of FWI95 that are not sufficiently close to the tail of the FWI distribution that they are well fit by a GEV distribution, as shown by the CI on the ERA5 return period when those values are excluded. These years were not excluded for the analysis, with that shown here to demonstrate that the infinite return period at all confidence levels is not affected by their inclusion.

### S4.1.2. Changes in Burned Area

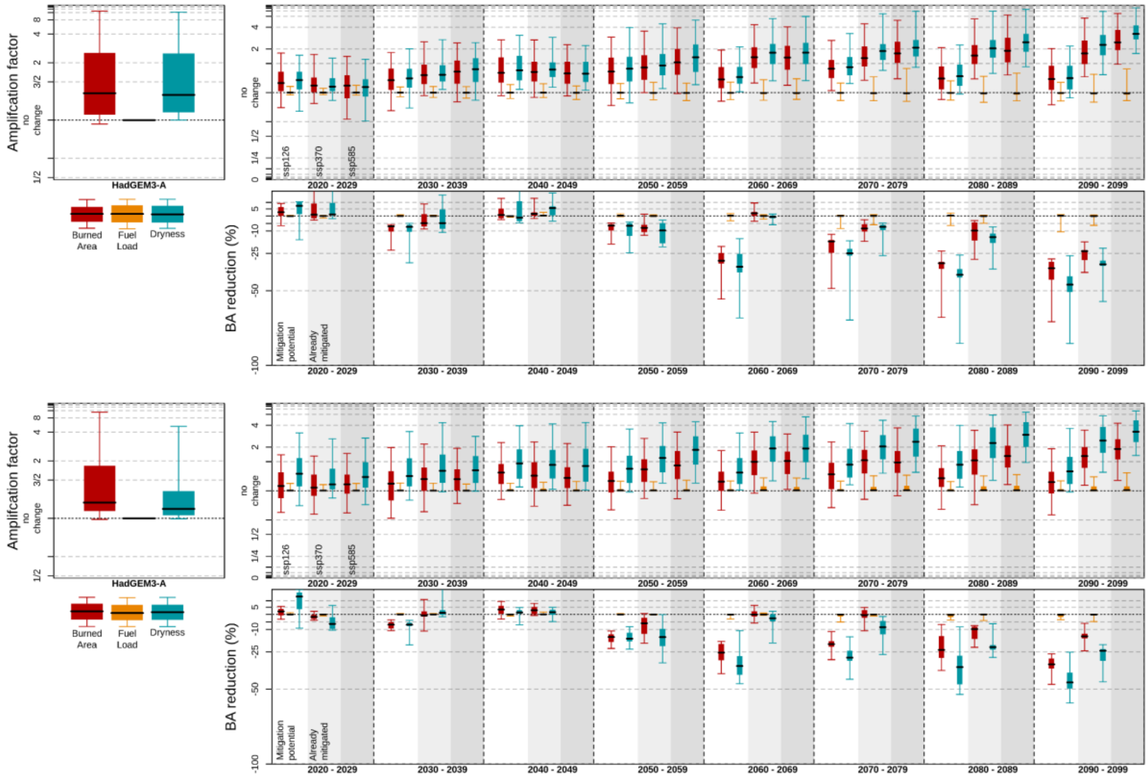


**Figure S16:** Top two panels per Figure 14 with future projections shown for each decade. Bottom two panels show attribution and projections for sub-regional extremes, i.e for grid cells with top 5% burned area.

**Table S10: Focal event burned area attribution and projection results** for present day and Shared Socioeconomic Pathway (SSP) scenarios. Colours denote likelihood based on IPCC definitions. Best estimate shown in bold, with 5-95[th] percentiles in brackets. Mitigation shows the % differences between SSP5-8.5 and SSP3-7.0 AF (in SSP3-7.0 columns) and SSP3-7.0 and SSP1-2.6 (in SSP1-2.6 columns), expressed as 100x (1-lower/high emissions BA).

| | | Present | SSP1-2.6 | | | SSP3-7.0 | | | SSP5-8.5 | | |
|---|---|---|---|---|---|---|---|---|---|---|---|
| | | | *2030s* | *2040s* | *2090s* | *2030s* | *2040s* | *2090s* | *2030s* | *2040s* | *2090s* |
| **BA** | *Probability Ratio* | **1.25** (0.66, 46.59) | **1.03** (0.93, 1.29) | **1.04** (0.92, 1.37) | **1.01** (0.87, 1.24) | **1.04** (0.94, 1.27) | **1.04** (0.94, 1.33) | **1.08** (0.94, 1.91) | **1.04** (0.93, 1.31) | **1.04** (0.94, 1.26) | **1.09** (0.9, 1.99) |
| | *Likelihood* | 84 | 69 | 70 | 56 | 78 | 77 | 82 | 73 | 75 | 79 |
| | *Amplification factor* | **1.25** (0.98, 15.08) | **1.18** (0.8, 2.12) | **1.33** (0.96, 2.8) | **1.15** (0.86, 2.15) | **1.27** (0.98, 2.46) | **1.31** (0.98, 2.56) | **1.78** (1.26, 6.84) | **1.32** (0.87, 2.28) | **1.3** (1, 2.28) | **2.33** (1.4, 11.36) |
| | *Likelihood* | 88 | 82 | 93 | 81 | 94 | 94 | 100 | 87 | 95 | 100 |
| | *Mitigation* | | **-7.96** (-6, -18.68) | **1.2** (11.38, -2.91) | **-35.55** (-29.34, -68.5) | **-1.99** (12.35, -1.99) | **0.23** (0.24, -1.78) | **-23.35** (-9.95, -34.65) | | | |
| | *Likelihood* | | 100 | 45 | 100 | 67 | 46 | 100 | | | |
| **Fuel** | *Amplification factor* | **1** (1, 1) | **1** (0.95, 1.08) | **1** (0.94, 1.09) | **1** (0.9, 1.12) | **1** (0.94, 1.07) | **1** (0.94, 1.1) | **0.99** (0.88, 1.27) | **1** (0.94, 1.08) | **1** (0.92, 1.09) | **0.99** (0.9, 1.32) |
| | *Likelihood* | 48 | 42 | 40 | 32 | 36 | 41 | 33 | 38 | 35 | 34 |
| | *Mitigation* | | **0.04** (1.38, -0.05) | **-0.03** (0.11, -0.03) | **0.32** (-11.57, 1.39) | **0** (-1.33, 0.2) | **0.24** (-0.06, 1.71) | **0.02** (-3, 0.74) | | | |
| | *Likelihood* | | 15 | 84 | 31 | 59 | 6 | 45 | | | |
| **Dryness** | *Amplification factor* | **1.26** (0.99, 14.75) | **1.23** (0.83, 2.23) | **1.38** (1.04, 3.02) | **1.19** (0.94, 2.15) | **1.28** (1.01, 2.85) | **1.34** (1.07, 4.07) | **2.17** (1.25, 17.43) | **1.37** (0.85, 2.35) | **1.32** (1.03, 2.9) | **3.1** (1.75, 25.89) |
| | *Likelihood* | 94 | 85 | 98 | 85 | 96 | 98 | 100 | 86 | 98 | 100 |
| | *Mitigation* | | **-6.92** (-2.1, -26.95) | **0.92** (15.72, 0.92) | **-44.93** (-87.64, -26.29) | **-3.75** (-8.1, 22.12) | **2.15** (-3.05, 33.11) | **-30.28** (-47.55, -20.78) | | | |
| | *Likelihood* | | 100 | 43 | 100 | 69 | 18 | 100 | | | |

| Virtually Certain | Very Likely | Likely | About as likely as not | Unlikely | Very Unlikely | Extremely Unlikely |
|---|---|---|---|---|---|---|
| >99% | >90% | >66% | 33-66% | <33% | <10% | <1% |

**Table S11: Sub-regional burned area extremes attribution and projection results**. Sub-regional extremes defined as the grid cells with top 5% BA. Otherwise as per Table S10

| | | Present | SSP1-2.6 | | | SSP3-7.0 | | | SSP5-8.5 | | |
|---|---|---|---|---|---|---|---|---|---|---|---|
| | | | *2030s* | *2040s* | *2090s* | *2030s* | *2040s* | *2090s* | *2030s* | *2040s* | *2090s* |
| **BA** | *Probability Ratio* | **1.35** (0.66, 94.74) | **0.97** (0.68, 1.1) | **0.96** (0.79, 1.17) | **0.95** (0.73, 1.14) | **0.98** (0.75, 1.15) | **1** (0.81, 1.2) | **1.02** (0.77, 1.39) | **0.98** (0.77, 1.16) | **1.02** (0.83, 1.19) | **1.06** (0.8, 1.46) |
| | *Likelihood* | 84 | 37 | 38 | 37 | 43 | 51 | 56 | 42 | 61 | 68 |
| | *Amplification factor* | **1.34** (0.99, 13.18) | **1.09** (0.67, 1.98) | **1.28** (0.93, 2.25) | **1.11** (0.67, 1.97) | **1.15** (0.78, 2.15) | **1.2** (0.9, 2.24) | **1.66** (1.07, 3.45) | **1.19** (0.88, 1.99) | **1.17** (0.84, 2.08) | **2.04** (1.2, 4.55) |
| | *Likelihood* | 91 | 66 | 88 | 68 | 74 | 86 | 97 | 82 | 79 | 99 |
| | *Mitigation* | | **-6.23** (-4.7, -15.75) | **2.58** (7.56, -3.61) | **-33.28** (-25.81, -46.12) | **-3.34** (6.34, -3.34) | **4.79** (0.05, 2.36) | **-19.27** (-12.51, -24.82) | | | |
| | *Likelihood* | | 100 | 19 | 100 | 86 | 2 | 100 | | | |
| **Fuel** | *Amplification factor* | **1** (1, 1) | **1** (1, 1.09) | **1** (1, 1.1) | **1** (1, 1.15) | **1** (1, 1.07) | **1** (1, 1.11) | **1** (1, 1.19) | **1** (1, 1.09) | **1** (1, 1.09) | **1.01** (1, 1.26) |
| | *Likelihood* | 48 | 93 | 96 | 87 | 92 | 92 | 90 | 87 | 92 | 96 |
| | *Mitigation* | | **0** (0.9, -0.08) | **0** (0.08, 0) | **-0.12** (-4.41, 0) | **0** (-0.99, 0.09) | **0.05** (0, 1.44) | **-0.26** (-4.53, 0) | | | |
| | *Likelihood* | | 32 | 46 | 99 | 35 | 18 | 100 | | | |
| **Dryness** | *Amplification factor* | **1.09** (1, 5) | **1.22** (0.93, 3.01) | **1.52** (1.05, 4.05) | **1.3** (0.97, 3.07) | **1.28** (0.96, 4.57) | **1.4** (1.02, 4.27) | **2.35** (1.24, 8.76) | **1.3** (0.99, 2.79) | **1.34** (0.98, 4.63) | **3.25** (1.77, 11.58) |
| | *Likelihood* | 96 | 90 | 99 | 93 | 93 | 97 | 100 | 91 | 93 | 100 |
| | *Mitigation* | | **-4.71** (-2.03, -19.78) | **4.82** (9.55, 4.82) | **-45.06** (-62.07, -22.8) | **0.55** (-3.79, 17.87) | **4.13** (-6.64, 7) | **-29.57** (-42.08, -18.27) | | | |
| | *Likelihood* | | 100 | 10 | 100 | 43 | 33 | 100 | | | |

### S4.1.3 Changes in Typical Fire Behaviour

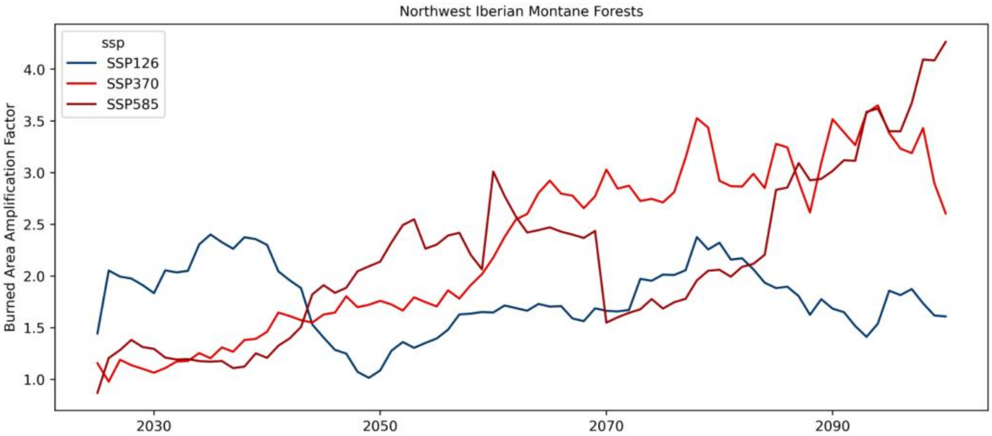


**Figure S17:** Future projections of burned area (BA) amplification factors (AF) from BuRNN for the 2025-2100 period, considering several Shared Socioeconomic Pathway (SSP) scenarios: SSP1-2.6 (blue), SSP3-7.0 (orange) and SSP5-8.5 (red).

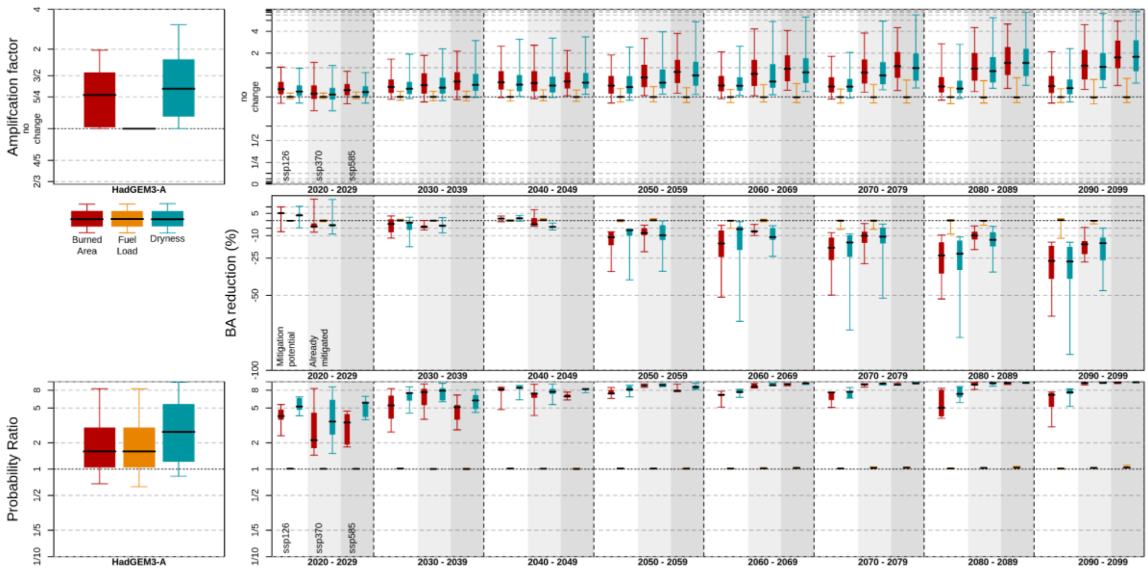


**Figure S18**: same as **Figure 14**, but for all simulated BAs to calculate amplification for the annual average burned area. Future calculations of amplification factor here use unconditioned BA as described in **Section 1.2.4.**

**Table S12: Annual average burned area attribution and projection results.** Otherwise, as per Table S10

| | | Present | SSP1-2.6 | | | SSP3-7.0 | | | SSP5-8.5 | | |
|---|---|---|---|---|---|---|---|---|---|---|---|
| | | | ***2030s*** | ***2040s*** | ***2090s*** | ***2030s*** | ***2040s*** | ***2090s*** | ***2030s*** | ***2040s*** | ***2090s*** |
| **BA** | ***BURNN*** | | 2.36 | 1.01 | 1.62 | 1.38 | 1.72 | 2.9 | 1.25 | 2.09 | 4.09 |
| | *Probability Ratio* | **1.25** (0.83, 12.47) | **3.7** (1.74, 12.61) | **11.31** (3.15, 16.21) | **6.67** (1.94, 8.69) | **8.39** (2.33, 38.84) | **7.47** (2.59, 35.43) | **60.92** (28.36, 94.83) | **3.43** (1.82, 6.62) | **5.96** (4.8, 8.45) | **>100** (47.91, >100) |
| | *Likelihood* | 83 | 100 | 100 | 100 | 100 | 100 | 100 | 100 | 100 | 100 |
| | *Amplification factor* | **1.27** (1, 1.97) | **1.15** (0.99, 1.87) | **1.18** (1, 2.45) | **1.14** (0.89, 2.07) | **1.17** (0.97, 2.04) | **1.2** (1, 2.67) | **1.52** (1.09, 5.31) | **1.24** (0.99, 2.07) | **1.22** (1.03, 2.22) | **1.98** (1.16, 7.58) |
| | *Likelihood* | 94 | 92 | 94 | 83 | 90 | 95 | 99 | 95 | 98 | 100 |
| | *Mitigation* | | **-2.03** (1.15, -12.18) | **-0.89** (0.92, -5.52) | **-25.15** (-15.65, -60.93) | **-4.95** (0.44, -4.95) | **-1.86** (0.17, -3.49) | **-23.15** (-6.3, -37.08) | | | |
| | *Likelihood* | | 77 | 68 | 100 | 95 | 71 | 100 | | | |
| **Fuel** | *Amplification factor* | **1** (1, 1) | **1** (0.96, 1.07) | **1** (0.95, 1.08) | **1** (0.93, 1.11) | **1** (0.96, 1.07) | **1** (0.95, 1.09) | **0.99** (0.93, 1.22) | **1** (0.95, 1.06) | **1** (0.95, 1.08) | **1** (0.93, 1.32) |
| | *Likelihood* | 49 | 39 | 39 | 33 | 38 | 41 | 35 | 35 | 35 | 38 |
| | *Mitigation* | | **0.07** (0.86, 0) | **0** (0.08, 0) | **0.09** (-9.68, 0.58) | **0.13** (0, 0.75) | **0.17** (0, 1.4) | **-0.06** (-10.74, 0.13) | | | |
| | *Likelihood* | | 11 | 62 | 42 | 6 | 2 | 82 | | | |
| **Dryness** | *Amplification factor* | **1.33** (1, 2.89) | **1.11** (0.98, 2.07) | **1.15** (1.01, 2.77) | **1.1** (0.93, 2.37) | **1.12** (0.98, 2.21) | **1.14** (1.01, 3.55) | **1.49** (1.11, 13.25) | **1.16** (1, 2.81) | **1.2** (1.04, 2.75) | **1.95** (1.2, 45.07) |
| | *Likelihood* | 98 | 91 | 96 | 81 | 92 | 96 | 100 | 95 | 99 | 100 |
| | *Mitigation* | | **-0.7** (-0.08, -15.76) | **0.33** (1.4, 0.33) | **-26.42** (-82.17, -15.34) | **-3.5** (-9.49, -1.51) | **-4.01** (-4.86, 21.19) | **-22.78** (-63.74, -7.72) | | | |
| | *Likelihood* | | 96 | 36 | 100 | 96 | 83 | 100 | | | |

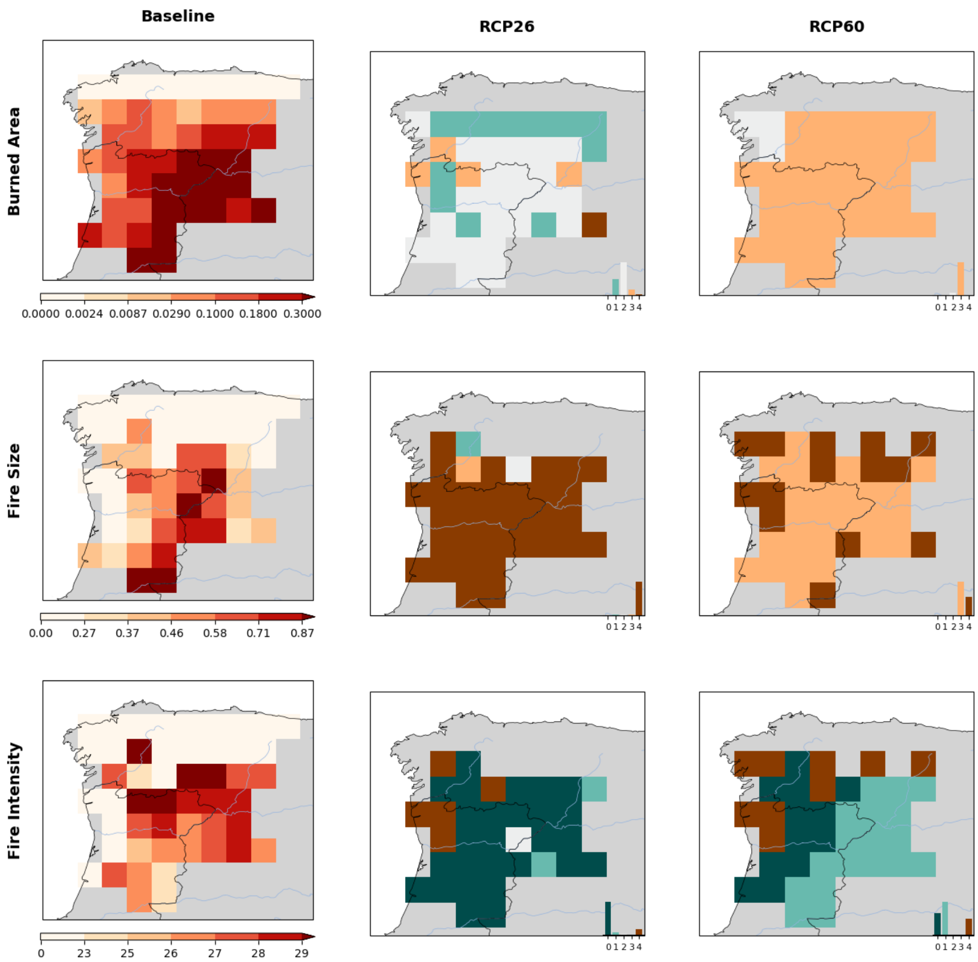


**Figure S19**. Projected changes in fire characteristics across ISMIP2b GMC future projections taken from Haas et al. (2026). The left column shows modelled baseline conditions for the 2010s, while the right columns show model agreement on the direction of change by 2100 under RCP2.6 (middle) and RCP6.0 (right). Colours indicate the number of models projecting an increase or decrease at each location (brown representing projected increases and blue representing projected decreases). . The accompanying histograms summarise the spatial extent of agreement by showing the fraction of the region where a given number of models agree on the direction of change. Rows correspond (top to bottom) to burned area, fire size, and fire intensity.

# S5. Focal Region 3: Chilean Temperate Forests and Matorral

## S5.1. Influence of Climate Change

### S5.1.1. Changes in Fire Weather

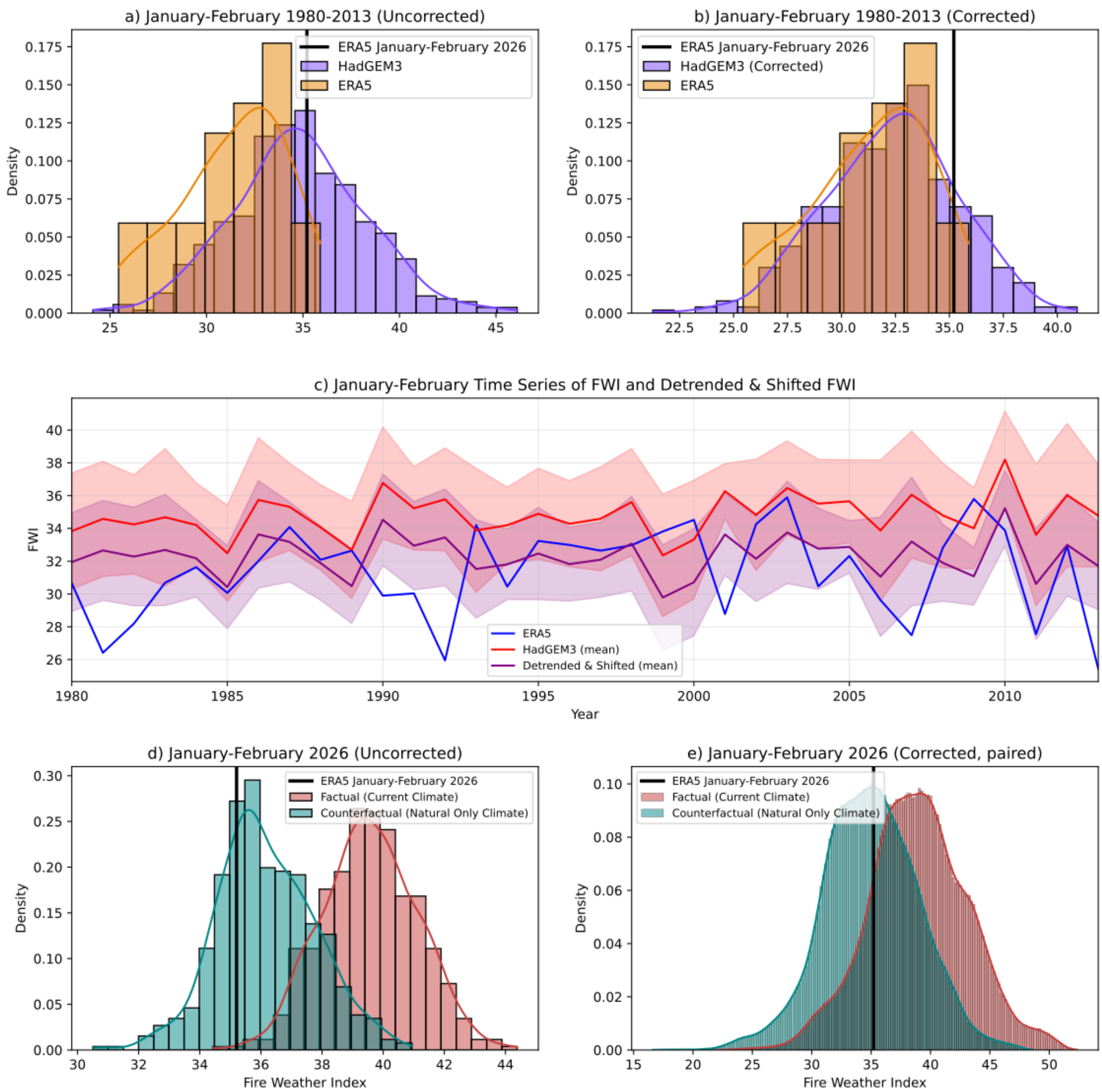


**Figure S20**: **HadGEM3-A Bias Correction.** (a): Histogram of uncorrected reanalysis (ERA5) and model (HadGEM3) results for FWI 95th percentile values for months July-August during the period 1980-2013. Black line denotes the ERA5 reanalysis value for the FWI 95th percentile value during the event period: **January-February 2026** (**FWI = 35.2**). **(b)**: Histogram of corrected model and reanalysis results for FWI 95th percentile values for period January-February 1980-2013.**(c):** Time-series of uncorrected (red), corrected (purple) model and reanalysis (blue) January-February FWI 95th percentile values for period 1980-2013. Solid Red and Purple lines denote 15 member mean, shading denotes 1std. **(d):** Uncorrected 525 member attribution ensemble histogram for FWI 95th percentile for 2020-2024, teal representing natural only climate, red denoting anthropogenically altered climate. **(e):** Bias corrected 7875 (525 * 15) member attribution ensemble histogram for 2020-2024, colours assignment unchanged.

**Figure S20** details the bias correction applied to the two attribution ensembles as summarised in **S1.2.1.** The uncorrected historical ensemble tends to overestimate the FWI at the higher end of the distribution. Nudges to the FWI95 value from the historical ensemble brought it into good alignment with the reanalysis values and when applied to the attribution ensemble generated sensible values in agreement with model synthesis. With respect to the reanalysis baseline period of 1980-2013, the FWI95 seen during the event in January-February 2026 was above average, and sits in the highest part of the historical distribution (panel a). During the baseline period the mean FWI95 from ERA5 was 31.4 versus the event value of 35.2. This represents a 12% increase over the climatology.

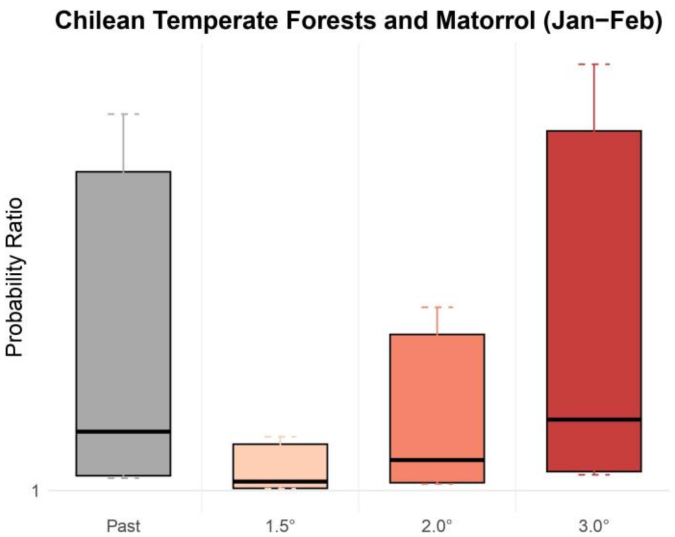


**Figure S21:** Probability Ratio (PR) estimates based on the comparison between (a) the past climate of 1850-1859 and the recent climate of 2017-2026, the recent climate of 2017–2026 and the period that global mean surface temperature (GMST) reached 1.5 °C, 2 °C and 3 °C for Chilean Temperate Forests and Matorral using FWI7X. Results are synthesised based on CanESM5, ACCESS-ESM1-5, and MPI-ESM1-2-LR from CMIP6 models with large (>10) climate ensembles. A 1000-sample non-parametric bootstrapping method is used to give uncertainty estimates for the FWI7X PRs. Bars show 5-95th confidence intervals (CIs), whiskers show 2.5th and 97.5th percentiles, and central values are shown by bold horizontal lines.

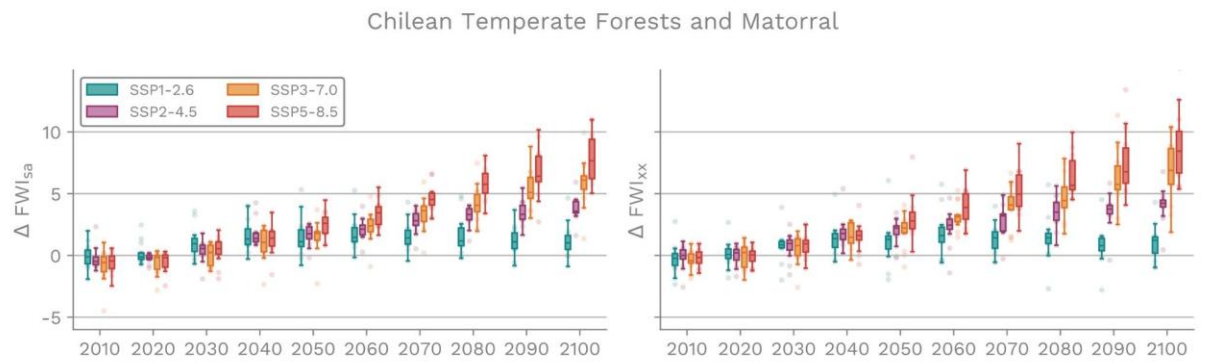


**Figure S22:** Projected changes in seasonal mean ($FWI_{sa}$; left) and annual maxima ($FWI_{xx}$; right) Fire Weather Index (FWI) for the Chilean Temperate Forests and Mattoral under CMIP6 SSP scenarios, with respect the reference period 2010-2020. Boxplots show the distribution across CMIP6 models for each decade, with coloured points indicating individual CMIP6 model results, while boxes represent the interquartile range (25th–75th percentiles).

### S5.1.2. Changes in Burned Area

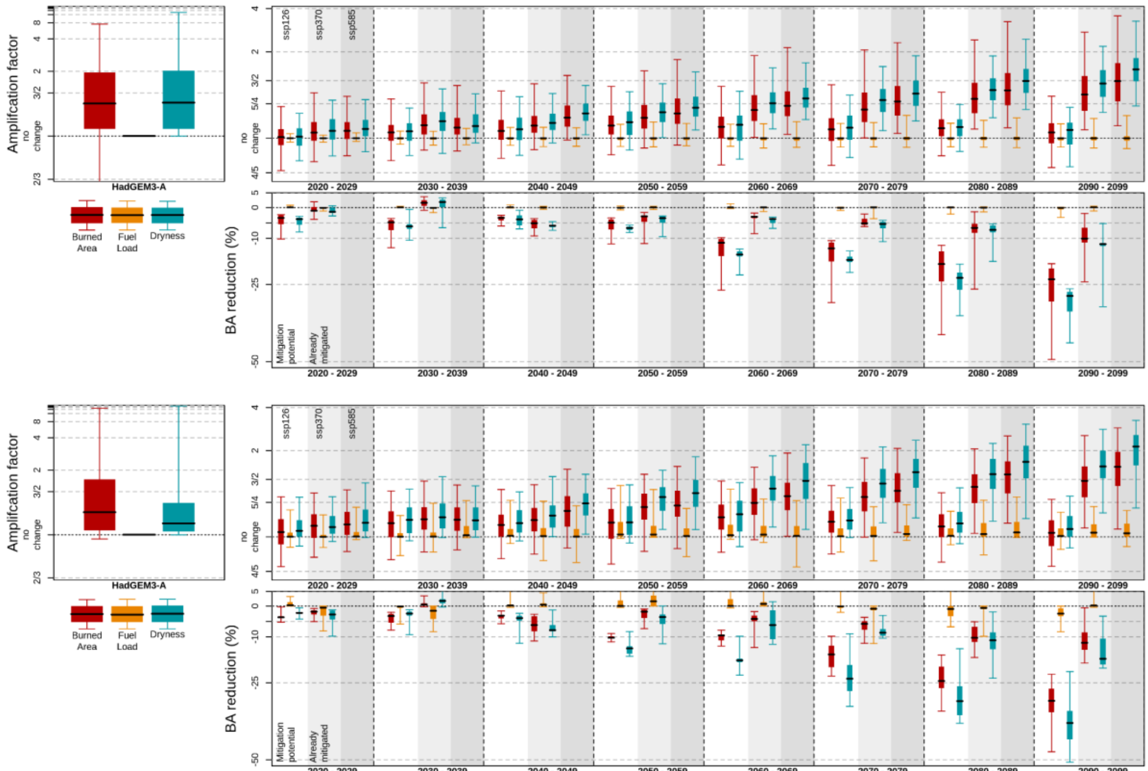


**Figure S23:** Top two panels per Figure 18 with future projections shown for each decade. Bottom two panels show attribution and projections for sub-regional extremes, i.e for grid cells with top 5% burned area.

**Table S13: Focal event burned area attribution and projection results** for present day and Shared Socioeconomic Pathway (SSP) scenarios. Colours denote likelihood based on IPCC definitions. Best estimate shown in bold, with 5-95$^{th}$ percentiles in brackets. Mitigation shows the % differences between SSP5-8.5 and SSP3-7.0 AF (in SSP3-7.0 columns) and SSP3-7.0 and SSP1-2.6 (in SSP1-2.6 columns), expressed as 100x(1-lower/high emissions BA).

| | | Present | SSP1-2.6 | | | SSP3-7.0 | | | SSP5-8.5 | | |
|---|---|---|---|---|---|---|---|---|---|---|---|
| | | | *2030s* | *2040s* | *2090s* | *2030s* | *2040s* | *2090s* | *2030s* | *2040s* | *2090s* |
| **BA** | *Probability Ratio* | **1.29** (0.84, 6.41) | **1.02** (0.93, 1.18) | **1.03** (0.93, 1.26) | **1.03** (0.92, 1.25) | **1.04** (0.96, 1.32) | **1.05** (0.96, 1.31) | **1.15** (1, 1.87) | **1.04** (0.96, 1.25) | **1.07** (0.98, 1.39) | **1.19** (1.02, 2.34) |
| | *Likelihood* | 93 | 68 | 75 | 69 | 81 | 82 | 96 | 82 | 90 | 96 |
| | *Amplification factor* | **1.36** (0.87, 7.37) | **1.03** (0.83, 1.28) | **1.04** (0.87, 1.33) | **1.03** (0.8, 1.36) | **1.08** (0.91, 1.48) | **1.07** (0.92, 1.42) | **1.34** (1.05, 2.64) | **1.07** (0.93, 1.45) | **1.13** (0.99, 1.63) | **1.47** (1.07, 3.17) |
| | *Likelihood* | 92 | 65 | 69 | 66 | 82 | 84 | 97 | 83 | 94 | 98 |
| | *Mitigation* | | **-5.77** (-4.46, -12.64) | **-3.45** (-3.09, -5.61) | **-24.1** (-18.57, -48.54) | **1.33** (2.6, 1.33) | **-5.33** (-0.03, -12.99) | **-9.04** (-2.47, -17.44) | | | |
| | *Likelihood* | | 100 | 99 | 100 | 24 | 100 | 100 | | | |
| **Fuel** | *Amplification factor* | **1** (1, 1) | **1** (0.97, 1.05) | **1** (0.96, 1.08) | **1** (0.95, 1.09) | **1** (0.96, 1.04) | **1** (0.95, 1.06) | **1** (0.94, 1.14) | **1** (0.97, 1.06) | **1** (0.96, 1.06) | **1** (0.94, 1.16) |
| | *Likelihood* | 46 | 35 | 37 | 39 | 34 | 37 | 40 | 40 | 38 | 41 |
| | *Mitigation* | | **0.06** (0.91, -0.08) | **0.07** (1.13, 0.07) | **0** (-3.03, 0.59) | **-0.24** (-1.6, -0.01) | **-0.03** (-0.45, 0.03) | **-0.1** (-1.96, 0.05) | | | |
| | *Likelihood* | | 6 | 17 | 48 | 100 | 88 | 71 | | | |
| **Dryness** | *Amplification factor* | **1.35** (1, 12.93) | **1.03** (0.87, 1.23) | **1.05** (0.9, 1.28) | **1.05** (0.83, 1.23) | **1.11** (0.91, 1.37) | **1.09** (0.97, 1.32) | **1.47** (1.17, 2.09) | **1.07** (0.96, 1.35) | **1.17** (1.02, 1.48) | **1.66** (1.26, 2.6) |
| | *Likelihood* | 96 | 63 | 71 | 70 | 82 | 89 | 100 | 88 | 96 | 100 |
| | *Mitigation* | | **-7.26** (-4.64, -11.1) | **-4.21** (-3.22, -4.21) | **-29.27** (-41.92, -26.33) | **2.76** (-4.55, 3.55) | **-6.47** (-8.72, -5.02) | **-10.58** (-19.16, -6.43) | | | |
| | *Likelihood* | | 100 | 100 | 100 | 27 | 100 | 100 | | | |

| Virtually Certain | Very Likely | Likely | About as likely as not | Unlikely | Very Unlikely | Extremely Unlikely |
|---|---|---|---|---|---|---|
| >99% | >90% | >66% | 33-66% | <33% | <10% | <1% |

**Table S14: Sub-regional burned area extremes attribution and projection results**. Sub-regional extremes, defined as the grid cells with the top 5% BA. Otherwise as per Table S13

| | | Present | SSP1-2.6 | | | SSP3-7.0 | | | SSP5-8.5 | | |
|---|---|---|---|---|---|---|---|---|---|---|---|
| | | | *2030s* | *2040s* | *2090s* | *2030s* | *2040s* | *2090s* | *2030s* | *2040s* | *2090s* |
| **BA** | *Probability Ratio* | **1.17** (0.88, 16.43) | **1.05** (0.91, 1.22) | **1.04** (0.89, 1.22) | **1.03** (0.9, 1.22) | **1.05** (0.93, 1.27) | **1.06** (0.94, 1.25) | **1.18** (1, 1.5) | **1.05** (0.92, 1.26) | **1.08** (0.93, 1.32) | **1.24** (1.03, 1.69) |
| | *Likelihood* | 83 | 74 | 71 | 69 | 78 | 84 | 95 | 78 | 81 | 97 |
| | *Amplification factor* | **1.2** (0.96, 44.13) | **1.08** (0.85, 1.37) | **1.07** (0.88, 1.34) | **1.04** (0.82, 1.29) | **1.13** (0.89, 1.47) | **1.11** (0.9, 1.43) | **1.49** (1.06, 2.29) | **1.09** (0.87, 1.4) | **1.16** (0.94, 1.55) | **1.65** (1.09, 2.76) |
| | *Likelihood* | 86 | 75 | 73 | 61 | 82 | 82 | 96 | 79 | 87 | 97 |
| | *Mitigation* | | **-3.98** (-3.01, -7.88) | **-3.94** (-1.89, -6.35) | **-30.29** (-22.48, -43.65) | **2.43** (5.33, 2.43) | **-4.17** (0.16, -7.18) | **-9.61** (-3.89, -17.25) | | | |
| | *Likelihood* | | 100 | 99 | 100 | 0 | 99 | 99 | | | |
| **Fuel** | *Amplification factor* | **1** (1, 1) | **1** (0.93, 1.2) | **1.01** (0.95, 1.26) | **1.01** (0.93, 1.16) | **1** (0.92, 1.15) | **1** (0.83, 1.2) | **1.03** (1, 1.26) | **1.01** (1, 1.27) | **1** (0.87, 1.21) | **1.02** (0.93, 1.2) |
| | *Likelihood* | 45 | 71 | 77 | 78 | 71 | 75 | 92 | 84 | 70 | 88 |
| | *Mitigation* | | **0.19** (4.27, -0.04) | **0.29** (10.86, 0.29) | **-3.1** (-8.71, -0.04) | **-2.04** (-10.41, -0.01) | **0.16** (-1.79, 1.36) | **0.84** (0.01, 9.16) | | | |
| | *Likelihood* | | 21 | 0 | 100 | 100 | 16 | 0 | | | |
| **Dryness** | *Amplification factor* | **1.1** (1, >100) | **1.1** (0.98, 1.31) | **1.09** (0.99, 1.38) | **1.07** (0.95, 1.31) | **1.13** (1, 1.5) | **1.16** (1.01, 1.52) | **1.75** (1.13, 2.61) | **1.08** (1, 1.42) | **1.23** (1.02, 1.63) | **2.1** (1.21, 3.27) |
| | *Likelihood* | 94 | 88 | 89 | 83 | 94 | 97 | 100 | 94 | 98 | 100 |
| | *Mitigation* | | **-2.96** (-1.28, -12.65) | **-5.66** (-2.42, -5.66) | **-39.11** (-49.87, -16.71) | **4.09** (-0.06, 7.7) | **-5.56** (-10.24, -1.37) | **-16.04** (-21.42, -6.74) | | | |
| | *Likelihood* | | 99 | 99 | 100 | 8 | 97 | 100 | | | |

### S5.1.3 Changes in Typical Fire Behaviour

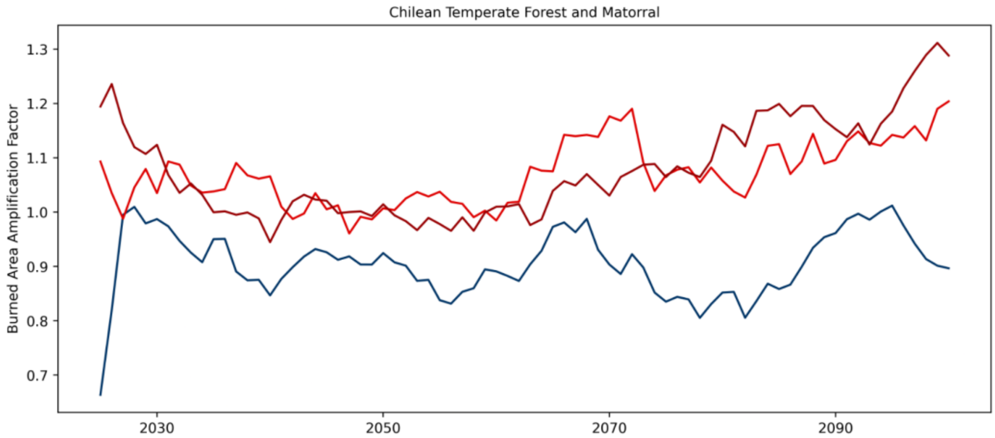


**Figure S24**: Future projections of burned area (BA) amplification factors (AF) from BuRNN for the 2025-2100 period relative to 2010-2019, considering several Shared Socioeconomic Pathway (SSP) scenarios: SSP1-2.6 (blue), SSP3-7.0 (orange) and SSP5-8.5 (red).

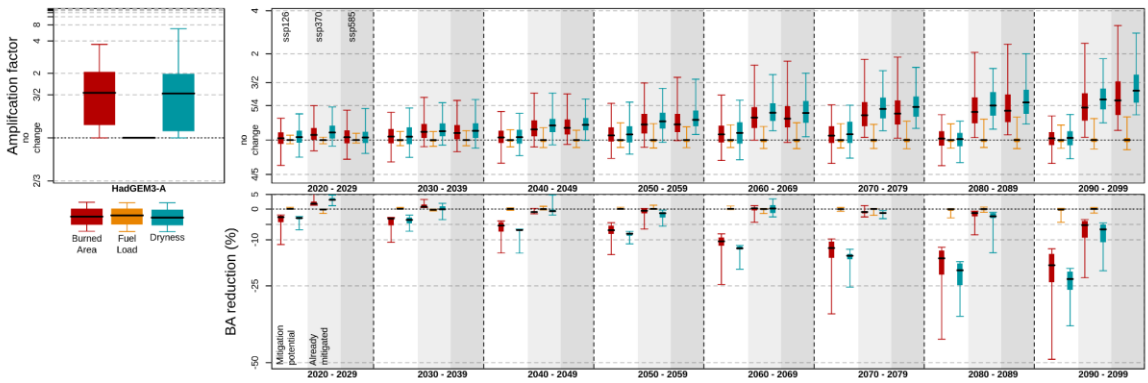


**Figure S25**: same as **Figure 18**, but for all simulated burned areas (BA) to calculate amplification factors (AF) for the annual average BA using ConFLAME. Future calculations of AF here use unconditioned BA as described in **Section 1.2.4.**

**Table S15: Annual average burned area attribution and projection results**. Otherwise, as per Table S13

| | | Present | SSP1-2.6 | | | SSP3-7.0 | | | SSP5-8.5 | | |
|---|---|---|---|---|---|---|---|---|---|---|---|
| | | | *2030s* | *2040s* | *2090s* | *2030s* | *2040s* | *2090s* | *2030s* | *2040s* | *2090s* |
| BA | ***BURNN*** | | 0.88 | 0.9 | 0.9 | 1.06 | 0.99 | 1.19 | 0.99 | 0.99 | 1.31 |
| | *Probability Ratio* | **1.48** (0.39, 8.64) | **1.07** (1.01, 1.12) | **1.05** (1.02, 1.23) | **1.04** (1.02, 1.07) | **1.08** (1.06, >100) | **1.21** (1.06, >100) | **2.8** (1.52, >100) | **19.78** (1.16, >100) | **1.09** (1.07, 1.78) | **11.16** (2.3, >100) |
| | *Likelihood* | 91 | 100 | 100 | 100 | 100 | 100 | 100 | 100 | 100 | 100 |
| | *Amplification factor* | **1.54** (1, 3.62) | **1.02** (0.9, 1.21) | **1.01** (0.87, 1.17) | **1.01** (0.85, 1.17) | **1.05** (0.97, 1.33) | **1.06** (0.97, 1.35) | **1.23** (1.02, 2.27) | **1.04** (0.95, 1.26) | **1.07** (0.96, 1.39) | **1.29** (1.04, 2.94) |
| | *Likelihood* | 94 | 64 | 62 | 59 | 85 | 85 | 97 | 79 | 88 | 97 |
| | *Mitigation* | | **-3.26** (-2.95, -10.31) | **-5.38** (-3.81, -14.94) | **-18.3** (-13.29, -48.51) | **1.21** (5.37, 1.21) | **-0.84** (-0.02, -2.18) | **-4.96** (-1.84, -22.35) | | | |
| | *Likelihood* | | 100 | 100 | 100 | 1 | 94 | 98 | | | |
| Fuel | *Amplification factor* | **1** (1, 1) | **1** (0.97, 1.05) | **1** (0.96, 1.06) | **1** (0.95, 1.1) | **1** (0.96, 1.03) | **1** (0.96, 1.08) | **1** (0.95, 1.15) | **1** (0.96, 1.06) | **1** (0.96, 1.08) | **1** (0.94, 1.15) |
| | *Likelihood* | 44 | 35 | 36 | 40 | 32 | 36 | 44 | 38 | 36 | 38 |
| | *Mitigation* | | **0.19** (1.23, 0) | **0.07** (0.48, 0.07) | **-0.07** (-3.41, 0.09) | **-0.2** (-1.68, -0.01) | **-0.02** (-0.2, 0.65) | **0.15** (-1.06, 0.79) | | | |
| | *Likelihood* | | 0 | 10 | 84 | 100 | 72 | 20 | | | |
| Dryness | *Amplification factor* | **1.52** (1, 6.43) | **1.02** (0.9, 1.25) | **1.02** (0.91, 1.16) | **1.01** (0.89, 1.15) | **1.06** (0.97, 1.33) | **1.08** (0.98, 1.34) | **1.3** (1.1, 1.94) | **1.05** (0.96, 1.28) | **1.09** (1, 1.31) | **1.4** (1.17, 2.8) |
| | *Likelihood* | 96 | 64 | 63 | 57 | 87 | 90 | 99 | 85 | 95 | 100 |
| | *Mitigation* | | **-3.75** (-2.47, -6.95) | **-5.88** (-5.28, -5.88) | **-22.86** (-41.1, -18.51) | **0.81** (0.46, 2.92) | **-1.02** (-2.21, 1.73) | **-6.81** (-26.15, -4.37) | | | |
| | *Likelihood* | | 98 | 100 | 99 | 3 | 91 | 100 | | | |

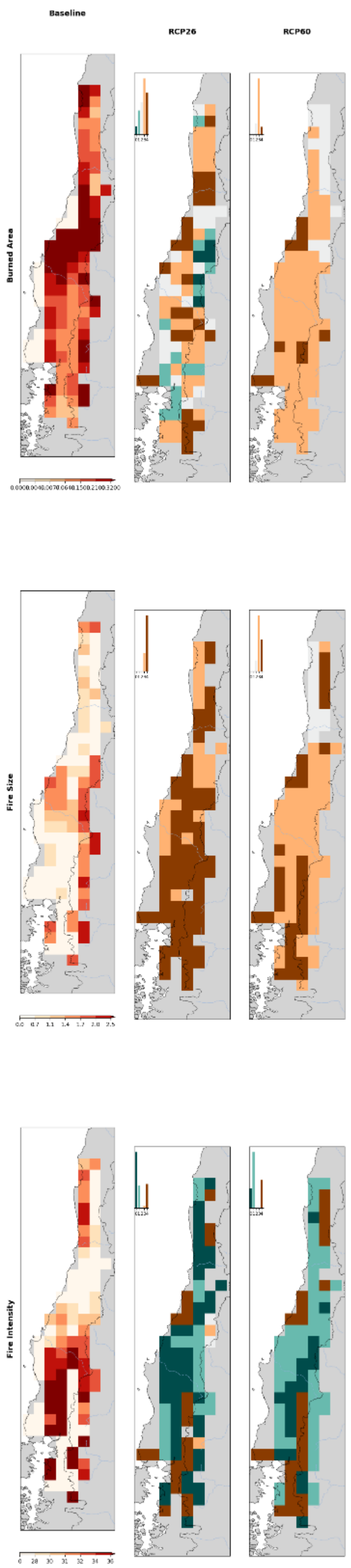


**Figure S26**. Projected changes in fire characteristics across ISMIP2b GCM future projections taken from Haas et al. (2026). The left column shows modelled baseline conditions for the 2010s, while the right columns show model agreement on the direction of change by 2100 under RCP2.6 (middle) and RCP6.0 (right). Colours indicate the number of models projecting an increase or decrease at each location (brown representing projected increases and blue representing projected decreases). The accompanying histograms summarise the spatial extent of agreement by showing the fraction of the region where a given number of models agree on the direction of change. Rows correspond (top to bottom) to burned area, fire size, and fire intensity.

# Supplementary References


Abatzoglou, J. T., Williams, A. P., and Barbero, R.: Global emergence of anthropogenic climate change in fire weather indices, Geophys. Res. Lett., 46, 326–336, https://doi.org/10.1029/2018gl080959, 2019.

Boussetta, S., Balsamo, G., Arduini, G., Dutra, E., McNorton, J., Choulga, M., Agustí-Panareda, A., Beljaars, A., Wedi, N., Munõz-Sabater, J., de Rosnay, P., Sandu, I., Hadade, I., Carver, G., Mazzetti, C., Prudhomme, C., Yamazaki, D., and Zsoter, E.: ECLand: The ECMWF Land Surface Modelling System, *Atmosphere*, 12, 723, https://doi.org/10.3390/atmos12060723, 2021.

Block, S., Emerson, J. W., Esty, D. C., de Sherbinin, A., Wendling, Z. A., et al. (2024): *2024 Environmental Performance Index*. New Haven, CT: Yale Center for Environmental Law & Policy. Available at: https://epi.yale.edu (last access: 03-January-2026)

Center for International Earth Science Information Network (CIESIN), Columbia University: Gridded Population of the World, Version 4 (GPWv4): Population Density, Revision 11, NASA Socioeconomic Data and Applications Center (SEDAC), https://doi.org/10.7927/H49C6VHW, 2018.

Ciavarella, A., Christidis, N., Andrews, M., Groenendijk, M., Rostron, J., Elkington, M., Burke, C., Lott, F. C., and Stott, P. A.: Upgrade of the HadGEM3-A based attribution system to high resolution and a new validation framework for probabilistic event attribution, Weather and Climate Extremes, 20, 9–32, https://doi.org/10.1016/j.wace.2018.03.003, 2018.

Copernicus Land Monitoring Service (CLMS): Leaf Area Index (LAI) 2014–present (raster 300 m), global, 10-daily, version 1, European Union's Copernicus Land Monitoring Service information, https://doi.org/10.2909/219fdc9f-616b-444b-a495-198f527b4722, last access: 3 March 2026.

Di Giuseppe, F., Pappenberger, F., Wetterhall, F., Krzeminski, B., Camia, A., Libertá, G., and San Miguel, J.: The potential predictability of fire danger provided by numerical weather 94 prediction, J. Appl. Meteorol. Climatol., 55, 2469–2491, https://doi.org/10.1175/jamc-d-15-0297.1, 2016.

Giglio et al., 2025 https://www.sciencedirect.com/science/article/pii/S0034425725004109

Haas, O., Prentice, I.C. and Harrison, S.P., 2026. Wildfires on a changing planet. Nature Communications, 17(1), p.1599.

Hersbach H, Bell B, Berrisford P, et al. The ERA5 global reanalysis. *Q J R Meteorol Soc*. 2020; 146: 1999–2049. https://doi.org/10.1002/qj.3803

Jolly, W. M., Cochrane, M. A., Freeborn, P. H., Holden, Z. A., Brown, T. J., Williamson, G. J., and Bowman, D. M. J. S.: Climate-induced variations in global wildfire danger from 1979 to 2013, Nat. Commun., 6, 7537, https://doi.org/10.1038/ncomms8537, 2015.

Jones, M. W., Abatzoglou, J. T., Veraverbeke, S., Andela, N., Lasslop, G., Forkel, M., Smith, A. J. P., Burton, C., Betts, R. A., van der Werf, G. R., Sitch, S., Canadell, J. G., Santín, C., Kolden, C., Doerr, S. H., and Le Quéré, C.: Global and regional trends and drivers of fire under climate change, Rev. Geophys., 60, https://doi.org/10.1029/2020rg000726, 2022.

Jones, M. W., Andela, N., Brambleby, E., Chuvieco, E., Giglio, L., Kaiser, J. W., Parrington, M., Qu, Y., Torres-Vázquez, M. Á., van der Werf, G. R., and Veraverbeke, S.: State of Wildfires 2025-26: Regional Summaries of Burned Area, Fire Emissions, and Individual Fire Characteristics for National, Administrative and Biogeographical Regions, Zenodo [data set]. https://doi.org/10.5281/zenodo.21262381, 2026.)

Kaplan, J.O., Bigelow, N.H., Prentice, I.C., Harrison, S.P., Bartlein, P.J., Christensen, T.R., Cramer, W., Matveyeva, N.V., McGuire, A.D., Murray, D.F. and Razzhivin, V.Y., 2003. Climate change and Arctic ecosystems: 2. Modeling, paleodata‐model comparisons, and future projections. Journal of Geophysical Research: Atmospheres, 108(D19). doi:10.1029/2002JD002559

Kelley, D. I., Burton, C., Di Giuseppe, F., Jones, M. W., Barbosa, M. L. F., Brambleby, E., McNorton, J. R., Liu, Z., Bradley, A. S. I., Blackford, K., Burke, E., Ciavarella, A., Di Tomaso, E., Eden, J., Ferreira,

I. J. M., Fiedler, L., Hartley, A. J., Keeping, T. R., Lampe, S., Lombardi, A., Mataveli, G., Qu, Y., Silva, P. S., Spuler, F. R., Steinmann, C. B., Torres-Vázquez, M. Á., Veiga, R., van Wees, D., Wessel, J. B., Wright, E., Bilbao, B., Bourbonnais, M., Gao, C., Di Bella, C. M., Dintwe, K., Donovan, V. M., Harris, S., Kukavskaya, E. A., N'Dri, A. B., Santín, C., Selaya, G., Sjöström, J., Abatzoglou, J. T., Andela, N., Carmenta, R., Chuvieco, E., Giglio, L., Hamilton, D. S., Hantson, S., Meier, S., Parrington, M., Sadegh, M., San-Miguel-Ayanz, J., Sedano, F., Turco, M., van der Werf, G. R., Veraverbeke, S., Anderson, L. O., Clarke, H., Fernandes, P. M., and Kolden, C. A.: State of Wildfires 2024–2025, Earth Syst. Sci. Data, 17, 5377–5488, https://doi.org/10.5194/essd-17-5377-2025, 2025.

Klein Goldewijk, K., Beusen, A., van Drecht, G. and de Vos, M. (2011), The HYDE 3.1 spatially explicit database of human-induced global land-use change over the past 12,000 years. Global Ecology and Biogeography, 20: 73-86. https://doi.org/10.1111/j.1466-8238.2010.00587.x

Kummu, M., Kosonen, M., and Sayyar, M. M.: Downscaled gridded global dataset for gross domestic product (GDP) per capita PPP over 1990–2022, *Sci. Data*, 12, 178, https://doi.org/10.1038/s41597-025-04487-x, 2025.

Li, X., Zhou, Y., Zhao, M. & Zhao, X. A harmonized global nighttime light dataset 1992–2018. *Sci. Data* **7**, 168 (2020) https://doi.org/10.1038/s41597-020-0510-y.

Liu, K., Wang, R., Schrijver, I., and Hoekstra, R.: Can we project well-being? Towards integral well-being projections in climate models and beyond, *Humanit. Soc. Sci. Commun.*, 11, 457, https://doi.org/10.1057/s41599-024-02941-6, 2024.

Lizundia-Loiola, J., Franquesa, M., Khairoun, A., Chuvieco, E. Global burned area mapping from Sentinel-3 Synergy and VIIRS active fires, Remote Sensing of Environment, Volume 282, 2022, 113298, ISSN 0034-4257, https://doi.org/10.1016/j.rse.2022.113298

Lizundia-Loiola et al., 2020 https://www.sciencedirect.com/science/article/pii/S0034425722004047

Lopez, P. A Lightning Parameterization for the ECMWF Integrated Forecasting System. *Mon. Weather Rev.* **144**, 3057–3075 (2016).

McNorton, J. R. and Di Giuseppe, F.: A global fuel characteristic model and dataset for wildfire prediction, *Biogeosciences*, 21, 279–300, https://doi.org/10.5194/bg-21-279-2024, 2024.

Meijer, J. R., Huijbregts, M. A. J., Schotten, K. C. G. J., and Schipper, A. M.: Global patterns of current and future road infrastructure, *Environ. Res. Lett.*, 13, 064006, https://doi.org/10.1088/1748-9326/aabd42, 2018.

Meiyappan, P., Jain, A.K. Three distinct global estimates of historical land-cover change and land-use conversions for over 200 years. *Front. Earth Sci.* **6**, 122–139 (2012). https://doi.org/10.1007/s11707-012-0314-2

Muñoz-Sabater, J., Dutra, E., Agustí-Panareda, A., Albergel, C., Arduini, G., Balsamo, G., Boussetta, S., Choulga, M., Harrigan, S., Hersbach, H., Martens, B., Miralles, D. G., Piles, M., Rodríguez-Fernández, N. J., Zsoter, E., Buontempo, C., and Thépaut, J.-N.: ERA5-Land: a state-of-the-art global reanalysis dataset for land applications, Earth Syst. Sci. Data, 13, 4349–4383, https://doi.org/10.5194/essd-13-4349-2021, 2021.

Pesaresi, M. & Politis, P. GHS-BUILT-S R2023A – GHS built-up surface grid, derived from Sentinel-2 composite and Landsat, multitemporal (1975–2030). Accessed 12 March 2025. https://doi.org/10.2905/9F06F36F-4B11-47EC-ABB0-4F8B7B1D72EA.

Qu, Y., Jones, M. W., Brambleby, E., Hunt, H. G. P., Pérez-Invernón, F. J., Yebra, M., Zhao, L., Moris, J. V., Janssen, T., and Veraverbeke, S.: A new global gridded lightning dataset with high spatial and temporal resolution, EGU General Assembly 2025, Vienna, Austria, 27 Apr–2 May 2025, EGU25-8351, https://doi.org/10.5194/egusphere-egu25-8351, 2025.

Soci, C., Hersbach, H., Simmons, A., Poli, P., Bell, B., Berrisford, P., et al. (2024) The ERA5 global reanalysis from 1940 to 2022. Quarterly Journal of the Royal Meteorological Society, 150(764), 4014–4048. Available from: https://doi.org/10.1002/qj.4803

Stocker, B. D., Wang, H., Smith, N. G., Harrison, S. P., Keenan, T. F., Sandoval, D., Davis, T., and Prentice, I. C.: P-model v1.0: an optimality-based light use efficiency model for simulating ecosystem gross primary production, Geosci. Model Dev., 13, 1545–1581, https://doi.org/10.5194/gmd-13-1545-2020, 2020.

Torres-Vazquez et al., 2026: Torres-Vázquez, M. Á., Segura-Garcia, C., Turco, M., Khairoun, A., Pettinari, M. L., Solano-Romero, E., García, M., Oliva, P., Jones, M. W., and Chuvieco, E.: MRBA60: Long-term consistent global burned area dataset from Sentinel-3 and MODIS products, Scientific Data, under revision.

Turco et al. (2026) Turco, M., Jones, M., & Di Giuseppe, F. (2026). State of Wildfires 2025-26: Anomalies in Extreme Fire Weather Days by Continent, Biome, Country, and Administrative Region (2026.0) [Data set]. Zenodo. https://doi.org/10.5281/zenodo.20757872

United Nations. *Human Development Report 2025.* Human Development Reports (2025). Accessed 30 October 2024. https://hdr.undp.org/content/human-development-report-2025.

Vitolo, C., Di Giuseppe, F., Barnard, C., Coughlan, R., San-Miguel-Ayanz, J., Libertá, G., and Krzeminski, B.: ERA5-based global meteorological wildfire danger maps, Sci. Data, 7, 216, https://doi.org/10.1038/s41597-020-0554-z, 2020.

van Wagner, C. E.: Development and structure of the Canadian forest fire weather index system, cabidigitallibrary.org, https://doi.org/10.5555/19910646918, 1987.

World Bank (2025): Worldwide Governance Indicators, 2025 Update, available at: https://www.worldbank.org/en/publication/worldwide-governance-indicators (last access: 04 January 2026).